

Article

Quasi-Static and Dynamic Tensile Behavior of Water-Bearing Sandstone Subjected to Microwave Irradiation

Pin Wang ^{1,2} , Tubing Yin ^{1,*}, Xibing Li ¹ and Heinz Konietzky ²¹ School of Resources and Safety Engineering, Central South University, Changsha 410083, China² Geotechnical Institute, TU Bergakademie Freiberg, 09596 Freiberg, Germany

* Correspondence: tubing_yin@mail.csu.edu.cn

Abstract: Microwave irradiation on rocks before excavation is an effective method to reduce equipment wear and energy consumption during mechanical cutting. Rock mass excavation is usually carried out in a water-rich environment and exposed to dynamic loads, thus understanding the coupled effects of water content and loading rate on the mechanical behavior of rocks under microwave radiation is essential. In this study, sandstone samples with five levels of water content (from oven-dried to water-saturated) were exposed to microwave irradiation at a power of 700 W for 10 min. Brazilian disc tests were conducted on sandstone samples after microwave radiation under both quasi-static and dynamic loading conditions. Test results revealed that, with the increase of the initial water content, the microwave heating capacity of the rock is significantly improved. The surface temperature of the saturated samples is approximately 1.38 times higher than that of the dry ones. Moreover, weight, P-wave velocity, quasi-static and dynamic tensile strength of the rock decrease, while porosity and damage factor exhibit a similar growth law. Before microwave irradiation, the average value of the P-wave velocity and the quasi-static tensile strength of sandstone were about $2521.3 \text{ m}\cdot\text{s}^{-1}$ and 4.65 MPa. However, after microwave treatment, when the initial water content was 2%, 3%, 4% and 5.4%, the P-wave velocity decreased by 6.1%, 9.8%, 16.4% and 30.2%, while that quasi-static tensile strength reduced by 9.2%, 16.7%, 30.6% and 48.9%, respectively. For water-saturated samples under microwave irradiation, the porosity increases from 13.02% to 18.12% (showing an increase of 39.2%), and the damage value rises to 0.51. In addition, the dynamic tensile strength shows a significant loading rate dependence, and as the initial water content increases, also the dynamic increase factor (DIF) increases. At a given loading rate, the energy dissipation decreases with the increase of the initial water content, which indicates that the presence of water cause more significant damage to the rock when subjected to microwave radiation. Scanning electron microscopy (SEM) results indicate that the internal damage of the rock after microwave radiation is dominated by intergranular cracks, and crack density increases with increasing initial water content of the samples. The underlying damage mechanisms of microwave radiation on water-bearing sandstone were interpreted with the theory of pore water pressure and structural thermal stresses.



Citation: Wang, P.; Yin, T.; Li, X.; Konietzky, H. Quasi-Static and Dynamic Tensile Behavior of Water-Bearing Sandstone Subjected to Microwave Irradiation.

Mathematics **2023**, *11*, 203. <https://doi.org/10.3390/math11010203>

Academic Editor: Yumin Cheng

Received: 23 October 2022

Revised: 25 December 2022

Accepted: 27 December 2022

Published: 30 December 2022

Keywords: water-bearing sandstone; microwave irradiation; porosity; dynamic tensile strength; energy dissipation; fracture mechanisms

MSC: 74L10



Copyright: © 2022 by the authors. Licensee MDPI, Basel, Switzerland. This article is an open access article distributed under the terms and conditions of the Creative Commons Attribution (CC BY) license (<https://creativecommons.org/licenses/by/4.0/>).

1. Introduction

The main problems faced by underground metal mines are efficient crushing of hard rock and long-term stability of the surrounding rock mass. The traditional drilling and blasting methods are gradually unable to meet the requirements of green and continuous mining in deep hard rock mines due to its intermittent and risky mining operations, low energy utilization rate, damage to the surrounding rock mass, and environmental pollution [1,2]. To address the problems mentioned above, methods are proposed such

as mechanical cutting [3,4], high-pressure water jet cutting [5], laser beam damaging [6], and high-temperature plasma rock breaking [7]. Mechanical cutting has the advantages of continuous operation, high construction quality, small excavation induced damage, increased safety, and economical operation. It has been strongly developed in the second half of the past century. In particular, the successful development of the shearer was the basis for the fully mechanized underground coal mining method, which has greatly improved the mining efficiency and operational safety. However, in metal mines, the wear of cutter head is severe due to the ore's high strength and abrasive nature, making it extremely difficult to crush the rock mechanically [8–11]. While researchers are committed to developing high-performance mining equipment to meet this challenge, they are also constantly looking for new rock-breaking technologies and auxiliary crushing methods.

Microwave-assisted rock breaking technology is a comprehensive thermal rock breaking technology. Compared with traditional heating technologies, microwaves heat up the rock internally, and the rock itself becomes a heating element causing thermal damage. It has the advantages of integral heating, fast heating rate, easy control of equipment, and avoids secondary pollution to the environment [12,13]. In recent years, constructors have shown increasing interest in microwave-assisted rock breaking technology. Substantial efforts have been made towards exploring the microwave heating effects on various rock types with respect to physical and mechanical behaviors, containing uniaxial compressive strength [13–17], tensile strength [13,14,18], point load strength [19], ultrasonic properties [20,21], fracture toughness [22,23], Cerchar abrasivity index [14], linear cutting forces [24], as well as tri-axial properties [16,25]. More detailed information on mentioned research is summarized in Table 1. It is universally accepted that microwave can effectively weaken rocks. The loss extent of the mechanical properties is primarily dependent on microwave intensity and exposure times, the dielectric properties of rocks, and the thermal expansion rate of the composing minerals [13,20]. Moreover, under the same irradiation energy, the combination of high heating power and low heating time is more effective to destroy rocks [15,20].

Above mentioned studies on the mechanical behavior of rocks are limited to quasi-static conditions. However, during the excavation process, due to the superposition of different methods such as cutting, punching, rolling, grinding, etc., rock masses are usually damaged and broken dynamically [26,27]. Under high strain rates, the mechanical behavior of rocks is significantly different from static loading [28,29]. The reactions of hard rocks to microwave radiation have also been studied at high loading rates. For example, Li et al. [30,31] conducted experimental research to study the dynamic properties of granite after microwave treatment, including uniaxial compressive strength, tensile strength, and fracture toughness. Results indicated that both original and irradiated granite samples exhibited a loading rate dependence, and microwave irradiation can facilitate the fragmentation of granite samples at a high loading rate. However, the only dry state of the sample was considered in these tests. For most engineering practice, due to the seepage effect of and aquifers in the mined-out area, rock mass excavation is usually carried out in a water-rich environment [32,33]. Generally, the laboratory tests use deionized water to investigate the effect of water content on the microwave heating of the rock. Studies have confirmed that the differential thermal expansion of mineral particles and the volumetric thermal expansion of water under microwave irradiation can cause crack evolution in rocks [34–36]. So far, limited studies have been conducted on microwave-induced reduction of mechanical attributes of rock materials considering different water content, and the high strain rate experiments on water-bearing rocks after microwave radiation is still not reported.

This paper aims to investigate the combined effects of water content and loading rate on the mechanical behavior of rocks under microwave radiation. By using the response surface methodology (RSM) and ANOVA for experimental design and data analysis [37]. A series of low-power microwave radiation tests on sandstone samples with different water content are performed. Some essential physical properties of sandstone samples, including surface temperature, porosity, and P-wave velocity, were determined. Furthermore, quasi-

static and dynamic tensile tests of the sandstone samples after microwave radiation were carried out using a servo-controlled testing machine and the Hopkinson pressure bar technique. Tensile strength and energy dissipation characteristics of the samples with different water content and loading rate were obtained and compared. The damage mechanisms of water-bearing sandstone under microwave radiation are discussed based on the theory of pore-water pressure and thermal stresses. Moreover, the sandstone used in this study has poor microwave absorbing capacities compared to some igneous rocks such as basalt, gabbro and diabase but has high hardness and abrasivity [13,21,38]. Therefore, the research results not only help us to deeply understand the combined effects of water content and loading rate on the mechanical behavior of rocks under microwave radiation but also provide theoretical evidence for engineering applications of the microwave-assisted mechanical rock-breaking technology, especially to provide possible solutions for the auxiliary breaking of rocks with poor microwave absorption capability.

Table 1. Summary of experimental studies on microwave treatment of rock materials.

Authors	Rock Type	Microwave Applicator	Microwave Power (kW)	Exposure Time (s)	Parameters Studied	Important Findings
Zheng et al. (2017) [20]	Gabbro	Single mode cavity	0.5–2 kW	30–120 s	T, V_p , Crack density	(1) Thermal gradients are huge when compared to conventional heating; (2) The overall V_p and the V_p in the middle of samples are reduced by up to 55% and 80%.
Hartlieb et al. (2018) [21]	Basalt, Diabase, Gabbro, Granite, Metasandstone, Cooper ore	Multimode cavity	3.2 kW	10–300 s	T, V_p	(1) The reaction to microwave irradiation strongly depends on the mineralogy or the water content of the rock; (2) Well-absorbing rocks melt and crack extensively as result of microwave irradiation.
Satish et al. (2006) [19]	Basalt	Multimode cavity	0.15 kW	60–360 s	T, I_s	(1) I_s decreases with the increase of irradiation time; (2) Visible macro cracking and splitting were observed on samples.
Shepel et al. (2018) [24]	Granite	Open ended waveguide	24 kW	30 s, 45 s	Cutting forces	34 s of microwave irradiation can significantly reduce cutting forces for granite, but the microwave penetration depth is limited.
Nekoovaght (2009) [14]	Granophyre, Granite, Gabbro, Gneiss, Basalt, Limestone	Multimode cavity	0.8 kW, 1.25 kW, 3 kW	15–240 s	T, UCS, BTS, CAI	(1) CAI and UCS decreased about 30% in almost all samples; BTS decreased up to 80% for the basalt samples; (2) Microwave-assisted rock excavation can improve the penetration rate and tool life of TBMs.
Ge and Sun (2021) [15]	Gabbro	Multimode cavity	0.9–6 kW	30–1500 s	T, UCS, AE	(1) When the heating power is greater than 3.3 kW, the damage to rock is more obvious; (2) High power and low heating time is more conducive to rock failure.
Hassani et al. (2016) [13]	Mafic norite, Granite, Basalt	Multimode cavity and open ended horn antenna	1.2 kW, 3 kW, 5 kW	10–120 s	T, UCS, BTS, Microwave penetration depth	(1) Smaller disc-shaped samples were heated more rapidly than larger cylindrical samples; (2) Wetting could increase the ability for the microwaves to induce cracks during 60 s exposure periods.
Kahraman et al. (2020) [18]	Granite, Syenite, Gabbro	Multimode cavity	1 kW, 2 kW, 6 kW	60–420 s	T, UCS, BTS	(1) UCS and BTS decrease with increasing power and exposure times; (2) Macro-cracks and local meltings could be observed on some samples after the treatment at 6 kW power.
Lu et al. (2022) [25]	Sandstone	Multimode cavity	1 kW	60–600 s	TCS, Brittle index	TCS and brittleness of the irradiated sandstone was significantly lower than that of the unirradiated sandstone.
Lu et al. (2020) [16]	Basalt	Multimode cavity	1 kW, 3 kW, 5 kW	10–300 s	T, UCS, TCS	TCS decreased linearly with exposure time, and the higher the confining pressure, the smaller the reduction in the strength of basalt.

Table 1. Cont.

Authors	Rock Type	Microwave Applicator	Microwave Power (kW)	Exposure Time (s)	Parameters Studied	Important Findings
Li et al. (2021) [22]	Granite	Multimode cavity	2 kW, 4 kW, 6 kW	30–150 s	T, K_{IC} , AE	K_{IC} decreased exponentially as the heating time, and is more sensitive to the higher microwave power.
Nejati et al. (2012) [23]	Basalt	Multimode cavity	1–5 kW	5–30 s	T, K_{IC}	K_{IC} decreases linearly with the increase of microwave energy while the crack density increases.
Wang et al. (2021) [39]	Granite	Multimode cavity	6 kW	90–270 s	Dynamic UCS, V_p , CT values, FSD	(1) CT value, V_p and dynamic UCS decreased with the increase of irradiation duration; (2) Microwave irradiation can facilitate the fragmentation of granite samples at low loading rates.
Yin et al. (2022) [40]	Basalt	Multimode cavity	1–4 kW	10–40 s	T, V_p , Dynamic BTS	There is a linear correlation between the dynamic tensile strength of the rock and the microwave energy input.
Chen et al. (2021) [41]	Shale	Multimode cavity	1 kW	0–50 s	NMR porosity, Permeability	Microwave heating can cause extensive fracturing and permeability enhancement in shale samples with moderate amounts of pore water.
Li et al. (2017) [42]	Coal	Multimode cavity	2 kW, 4 kW, 6 kW, 8 kW, 10 kW	30 s	NMR porosity, Permeability, V_p	(1) The fracture volume and coal permeability increase while the V_p decreases with increasing water contents; (2) When the water content is above 6%, the porosity increases by around 98–211%.
Zhao et al. (2020) [36]	Sandstone	Multimode cavity	0.5 kW	60–480 s	T, PSD	(1) The heating curves of saturated sandstones can be divided into 3 stages; (2) Water-bearing sandstones are more likely to burst with low rock strength, low permeability, high saturation degree and high microwave power.
Peinsitt et al. (2010) [34]	Basalt, Granite, Sandstone	Multimode cavity	3 kW	10–300 s	T, UCS, V_p	(1) V_p decreases with the increase of radiation time whereas UCS fluctuated; (2) Water-saturated sandstones burst on reaching temperatures slightly above 100 °C.

Note: T-Temperature; UCS-Uniaxial compression strength; BTS-Brazilian tensile strength; TCS-Triaxial compression strength; CAI-Cerchar abrasivity index; I_s -Point load strength index; V_p -P-wave velocity; K_{IC} -Fracture toughness; FSD-Fragment size distribution; PSD-Pore size distribution.

2. Material and Experimental Methods

2.1. Material Description

The sandstone used for this study was taken from an underground metal mine in Changsha City, Hunan Province, China. The entire sandstone block is brown-red, and there are no apparent cracks on the sample’s surface. In order to determine the mineral composition and structure of the rock, thin sections of sandstone were stained with Alizarin Red solution, and they were observed under plane-polarized light with an optical microscope, as shown in Figure 1a. The sandstone has a silty fine sand structure. The primary type of cementation is porous cementation, and basal cementation is partially seen. The main mineral components are quartz, feldspar, calcite, and muscovite, as well as a small amount of hematite and chlorite. The size of minerals ranges from 0.03–0.5 mm, but a few larger particles can reach up to 0.6 mm. By X-ray diffraction analysis technology the specific mass fraction of each mineral component was determined, as shown in Figure 1b.

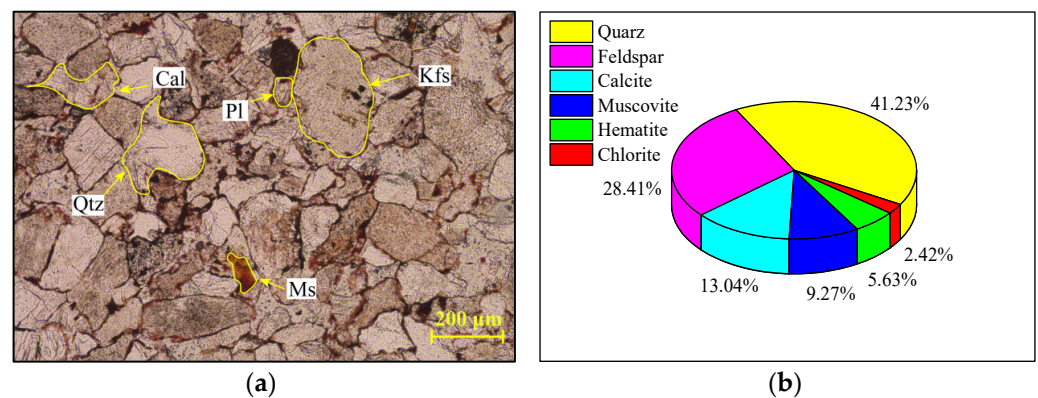


Figure 1. Mineral composition: (a) optical microscope image of sandstone and (b) content of minerals. (Qtz-quartz; Kfs-Potash feldspar; Pl-plagioclase; Cal-calcite; Ms-muscovite).

2.2. Sample Preparation

In this study, Brazilian tests was chosen to determine the quasi-static and dynamic tensile strength. The sample preparation process follows the recommendations of the International Society of Rock Mechanics (ISRM) [43]. A diamond drill bit with an inner diameter of 50 mm was used to obtain core samples from the sandstone block. All core axes are consistent to avoid influence due to the rock anisotropy on its physical and mechanical properties. A rock cutter was used to slice the cylindrical cores into Brazilian disc samples with an average thickness of 25 mm. After that, a double-sided grindstone machine was adopted to carefully polish each sample’s end surface and circumference to ensure that the non-parallelism between the two ends of the sample is less than 0.025 mm, non-perpendicularity between the circumference and the end surface is less than 0.25°. All processed samples were dried in a vacuum drying oven at 105 °C for 48 h. Then, samples with significant deviations in respect to weight, wave velocity and porosity are eliminated. Before microwave radiation tests, we also conducted a series of preliminary tests on dried samples to determine the primary physical and mechanical parameters of the sandstone, as listed in Table 2.

Table 2. Physical and mechanical properties of the sandstone (mean values and standard deviation).

	$\rho(\text{kg}\cdot\text{m}^{-3})$	$P(\%)$	$A_w(\%)$	$C_p(\text{m}\cdot\text{s}^{-1})$	$\sigma_c(\text{MPa})$	$\sigma_{st}(\text{MPa})$	$E_s(\text{GPa})$
Mean values	2336.2	13.3	5.43	2521.3	68.9	4.65	6.47
Standard deviation	± 2.17	± 0.25	± 0.14	± 37.5	± 1.87	± 0.11	± 0.19

Note: ρ : Density; P : Porosity; A_w : Water absorption; C_p : P-wave velocity; σ_c : Uniaxial compression strength; σ_{st} : Static tensile strength; E_s : Elastic modulus.

In order to study the influence of initial water content on the damage of sandstone samples under microwave radiations, the vacuum-dried sandstone samples were completely immersed in deionized water with a temperature equal to 25 °C and a pH value of 7 for 48 h, as shown in Figure 2a. The main reason for using deionized water is to avoid the rotation and friction of other ions under microwave radiation, producing thermal effects and affecting the test results. During the soaking process, the samples were taken out and weight was determined at intervals of one hour until the sample weight remains unchanged. The water content of the samples at different soaking times can be calculated by the variation of sandstone weight:

$$w = \frac{m_w - m_d}{m_d} \tag{1}$$

where, w is the moisture content of the sample, %; m_d and m_w are the dry and wet weight of the sample after soaking for a certain period, g. Figure 2b shows the variations of the moisture content of the sandstone samples with soaking time. The moisture content of the sandstone increases rapidly during the initial stage, and the growth rate of water content slows down with increasing soaking time. After the sample is immersed in water for about 28 h, no significant change in water content is observed. At this time, the sandstone is fully saturated.

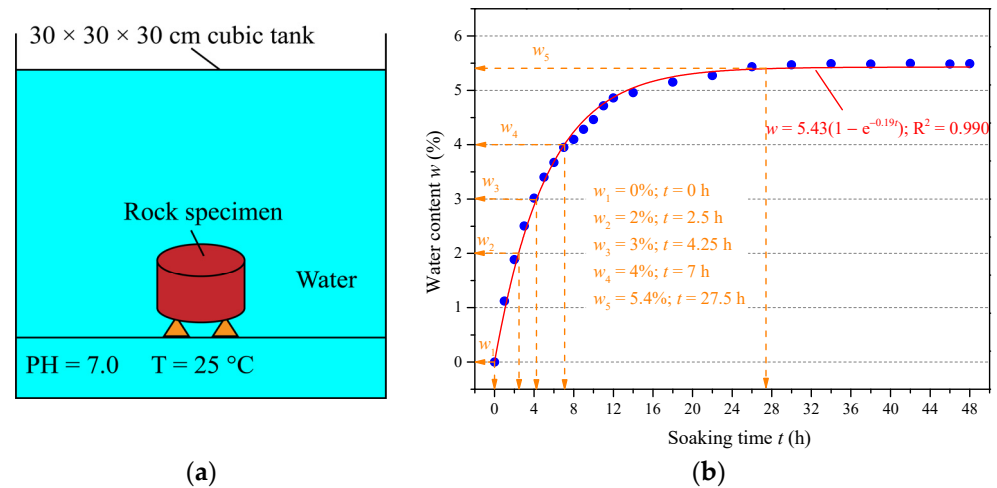


Figure 2. (a) schematic diagram of water immersion treatment method, (b) variation of water content vs. soaking time.

In this study, the OriginPro software was used to perform multivariate statistical regression analysis on the physical and mechanical variables of sandstone. This software was selected due to its strength that a user could get an optimum fitting equation with a high fault-tolerant rate and high searching rate by its “Model Comparing” function. After regression analysis, the “goodness of fit” can be used to evaluate the validity of the fit. Generally, R-squared (R^2), also known as the coefficient of determination, could be used to assess the correlation between the fitted curve and the test data; the value of R^2 ranges from 0 to 1, and a higher value indicates a better fit. By regression analysis using OriginPro software, the variation of water content and soaking time are related by the following equation:

$$w = w_s(1 - e^{-at}) = 5.43(1 - e^{-0.19t}); \quad R^2 = 0.990 \tag{2}$$

where, w_s is the saturated water content of the sample, %; t is the soaking time of the sample, h; and a is the fitting parameter.

According to Figure 2b and Formula (2), a sample with a specific moisture content can be easily prepared. In this study, all samples are divided into five groups, and each

group consists of six samples for static and dynamic splitting tests. The water content of the sandstone samples was fixed to 0%, 2%, 3%, 4%, and 5.4%, and the corresponding immersion times were about 0 h, 2.5 h, 4.25 h, 7 h, and 27.5 h. After preparing the sandstone samples with different water content, samples were sealed by a thin plastic film to protect them from moisture exchange in the atmosphere. However, when samples are placed in a microwave field, the plastic film must be removed.

2.3. Test Set-Up and Data Acquisition

2.3.1. Microwave Heating Equipment

The purpose of this research is to characterize the influence of water content on the tensile properties of sandstone subjected to microwave radiations; therefore, the integrity of the sandstone samples must be ensured before the mechanical tests. Previous studies have shown that high-power microwave radiation may cause rock bursting and destruction [35,36]. Therefore, in this study, water-bearing sandstone samples were subjected to microwave heating using a 700 W domestic microwave oven at a frequency of 2.45 GHz, which corresponds to an approximate wavelength of 120 mm, as shown in Figure 3a. The domestic microwave oven used in this study is a typical multi-cavity microwave oven, and the bottom of the microwave oven is equipped with a glass turntable to ensure uniform heating of the sample. All samples are irradiated in the microwave oven for 10 min. The surface temperature of the samples were measured with a full-color infrared thermal imager every 30 s (see Figure 3b), and the weight change of the sample was also recorded. For doing the measurements the samples were taken out of the oven for just a few seconds so that surface temperature variations of the samples are negligible. A detailed flowchart illustrating the microwave treatment and experimental procedure can be seen in Figure 4.

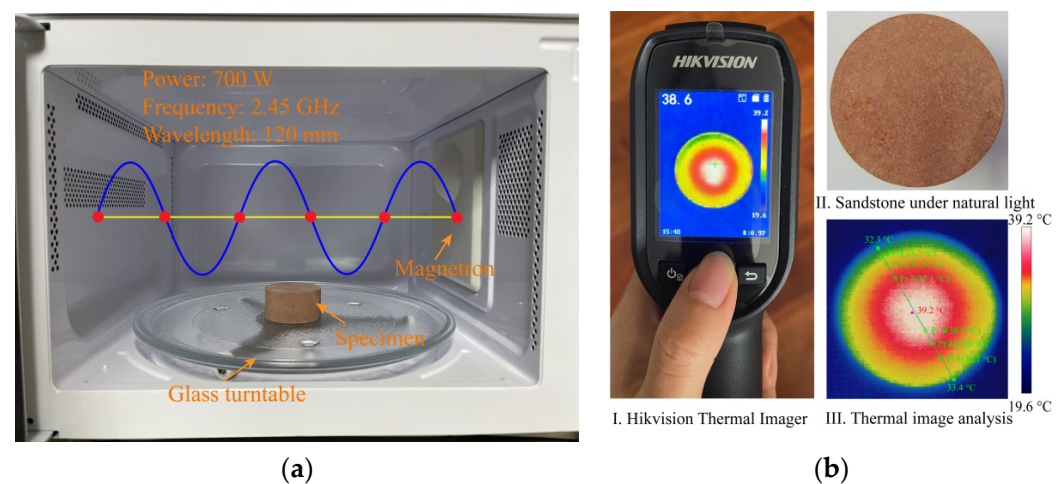


Figure 3. (a) microwave oven and (b) thermal analysis of sandstone.

2.3.2. Quasi-Static Brazilian Tests

Quasi-static Brazilian disc tests were conducted on a MTS hydraulic servo testing machine. The sandstone disc was compressed diametrically under displacement-controlled loading by a flat load platen without any cushion strips or loading jaws on the sample, consistent with the dynamic splitting tests. The loading rate was 10^{-4} mm/s, and the MTS testing system recorded vertical load and displacement. According to the principle of the Brazilian test, a compressive load can generate a tensile stress perpendicular to the diameter of the disc in the sample [44]. When the failure occurs at the point of maximum tensile stress (i.e., at the center of the disk), the tensile strength can be calculated as:

$$\sigma_{st} = \frac{2F_{\max}}{\pi DB} \quad (3)$$

where, σ_{st} is the static tensile strength of the sample, MPa; F_{max} is the maximum load, N; D and B are the diameter and thickness of the sample, mm; respectively.

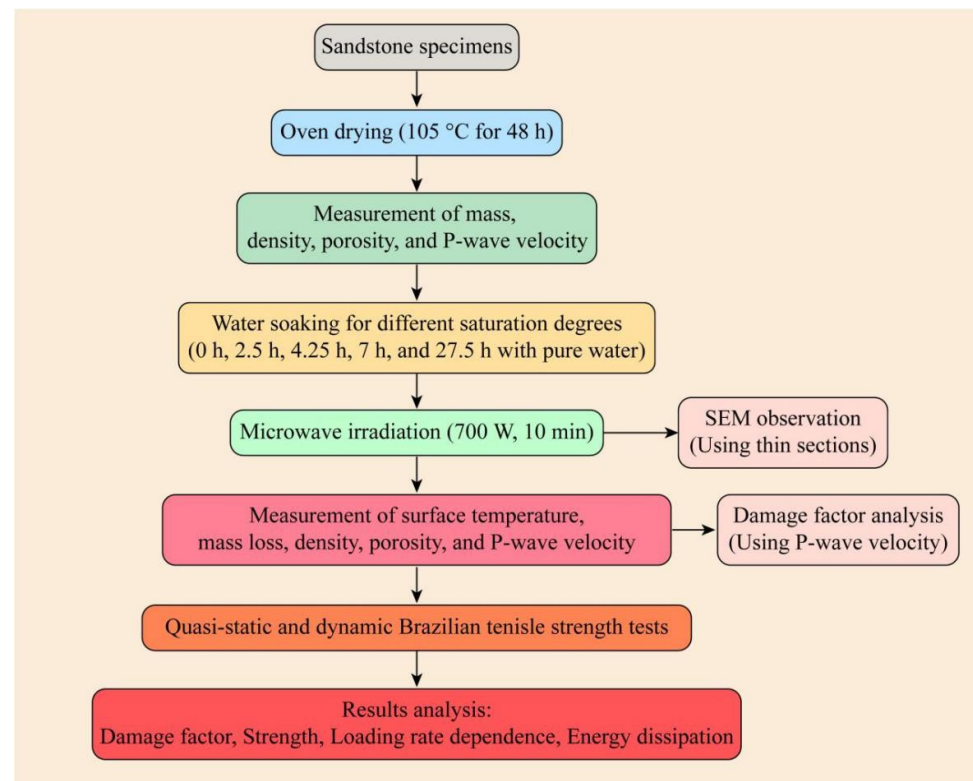


Figure 4. Flowchart of the microwave treatment and experimental procedure.

2.3.3. Split Hopkinson Pressure Bar System

The dynamic Brazilian split tests were carried out on a modified split Hopkinson pressure bar (SHPB) system, which can realize the loading of rock-like materials under medium and high strain rate conditions [45]. The experimental device consists of a launch tube, striker, incident bar, transmission bar, energy absorption bar, and data acquisition system, as shown in Figure 5a,b. During the test, the sandstone disc was sandwiched between the incident bar and the transmission bar diametrically. The striker in the launch tube was driven by high-pressure nitrogen to hit the incident bar and generate a one-dimensional compressive stress pulse in the incident bar, that is, the incident wave. The incident wave propagates through the sample, a reflected tensile wave and a transmitted compression wave are generated. Strain gauges are attached to the middle of the incident bar and the transmission bar to record the stress waves. A high-speed camera was adopted to capture the dynamic fracture process of the sample with a shooting frame rate of 125,000 fps. The camera is triggered by the incident wave to ensure that the strain signal is synchronized with the image acquisition.

Unlike the traditional SHPB equipment, the modified SHPB adopts a cone-shaped striker in the launch tube to eliminate the dispersion effect of the stress wave and the P-C oscillation [46]. Figure 5c presents a typical loading stress wave recorded by the strain gauges on the elastic bars. The signals in Figure 5c are very smooth, and the incident wave has an approximate half-sine wave shape. Additionally, the front edge of the incident wave rises slowly, effectively avoiding the premature rupture of the sample in the loading section.

The SHPB system should be calibrated without mounting the sample, and the testing accuracy of the equipment is 0.01 MPa. The stress balance at both ends of the sample

is the fundamental premise for the effectiveness of the SHPB test. According to the one-dimensional stress wave propagation theory of the SHPB test, the forces at the two ends of the sample are [47]:

$$F_1(t) = E_e A_e [\varepsilon_I(t) + \varepsilon_R(t)] \tag{4}$$

$$F_2(t) = E_e A_e \varepsilon_T(t) \tag{5}$$

where, E_e and A_e are the elastic modulus and cross-sectional area of the elastic bar, Gpa and m^2 ; $\varepsilon_I, \varepsilon_R$ and ε_T are the incident, reflection, and transmission strains, respectively. Figure 6a presents a typical dynamic force balance curve of an SHPB test of a sandstone sample. It can be found that during the process of dynamic loading, the curves of superimposed stress and the transmission stress at both ends of the sample basically coincide, which indicates that the loading force at both ends of the sample is almost the same (i.e., $F_1 = F_2$). Therefore, the inertial effect during the dynamic loading process can be ignored, and the quasi-static theory can be used to analyze the force conditions of the sandstone samples [47,48]. The formula for calculating the dynamic tensile strength of disc samples can be expressed as:

$$\sigma_{dt}(t) = \frac{2F(t)}{\pi DB} = \frac{E_e A_e}{\pi DB} [\varepsilon_I(t) + \varepsilon_R(t) + \varepsilon_T(t)] \tag{6}$$

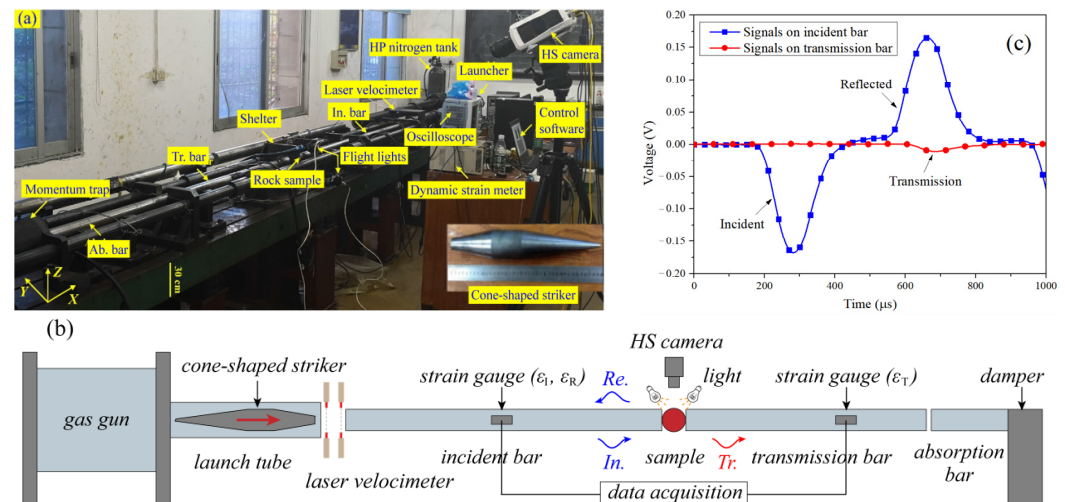


Figure 5. Photographic (a) and schematic diagram (b) of the modified split Hopkinson pressure bar system, and (c) typical data recording result.

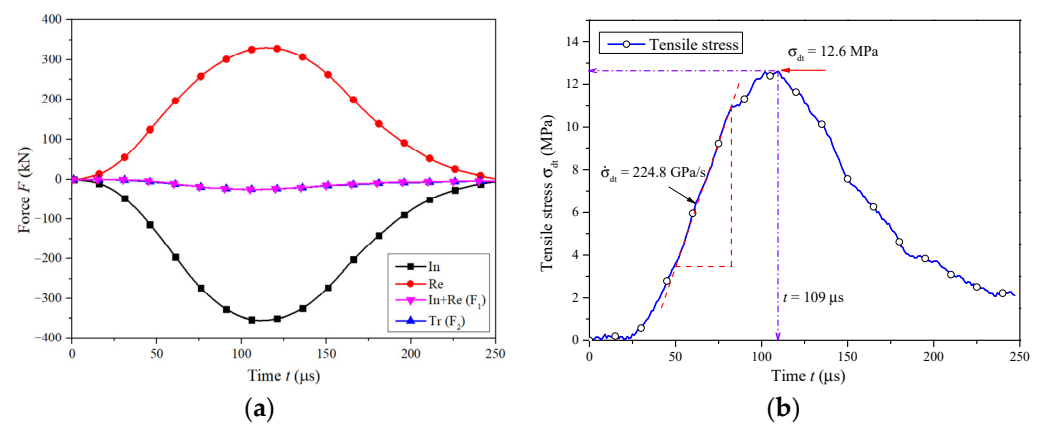


Figure 6. Verification of the dynamic force balance at both ends of the sample (a) and the determination of the loading rate (b).

During the dynamic loading process, the impact velocity of the striker can be controlled by adjusting the gas pressure in the air gun so as to achieve different loading rates. Referring

to the studies of Zhang et al. [49], we defined the slope of the linear segment of the tensile stress curve before reaching the peak as actual loading rate, as shown in Figure 6b. It can be seen from Figure 6b that the dynamic tensile strength of a typical sample is 12.6 MPa, and the loading rate is about 224.8 GPa/s.

3. Results and Analysis

3.1. Physical Damage Induced by Microwave Irradiation

3.1.1. Temperature Variations and Weight Loss

Microwave heating mainly uses the principle of dielectric loss to convert microwave energy into heat energy. The generated heat is related to the rock-forming minerals and their dielectric properties. Figure 7 shows the dielectric constants of pure water and sandstone's main rock-forming minerals for 2.45 GHz microwave frequency and room temperature [50,51]. Except for hematite, the dielectric constants of all other rock-forming minerals are less than 10. Even though the dielectric constant of hematite is 18.3, its content only accounts for 5.63% of the total mass (see Figure 1b), which results in a relatively low microwave sensitivity of the sandstone. In addition, the dielectric constant of water is significantly greater than that of the sandstone minerals (factor of 4 to 20). Therefore, when the water content increases, dielectric properties will inevitably increase, and the microwave heat conversion capability of the rock will also change accordingly, which ultimately leads to a temperature variation in the rock.

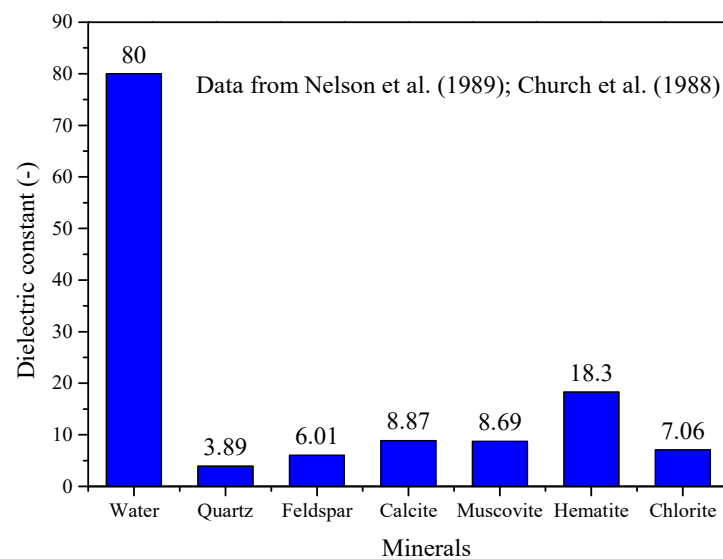


Figure 7. Dielectric constants of pure water and sandstone's main rock-forming minerals [50,51].

Figure 8 shows the surface temperature of sandstone samples with different water content under microwave radiation. In order to better reflect the temperature variations, the scale value of the temperature distribution cloud map is unified, and the highest temperature on the surface of the sample is marked. With increasing of initial water content and extension of duration of microwave radiation, the surface temperature of the samples increases, which indicates that the presence of water increases the dielectric properties of the sandstone and the microwave heating capacity. In addition, due to the effects of convective heat transfer and moisture evaporation, most of the sample surfaces present a temperature gradient with higher temperatures at the center and lower at the edge of the sample. However, it is worth noting that when the initial water content is 2% and 3%, and the duration of microwave radiation is 60 s and 180 s, the highest temperature occurs at the edge of the sample, and a colder zone is formed at the center. The main reason for this phenomenon is that the pore water concentrate in the outer layer of the sample in case of low water content. As a strongly polar molecule, water can take the lead in absorbing microwaves and converting them into heat energy, causing the edge temperature

of the sample to be higher than the center temperature. As the duration of microwave radiation increases, the moisture at the edge of the sample evaporates and takes heat away. In summary: under the combined effects of water evaporation, heat transfer in the rock, and the convective heat exchange between the sample surface and the surrounding air, the sample surface presents the typical temperature distribution characteristics of high temperature at the center and low temperature at the edges.

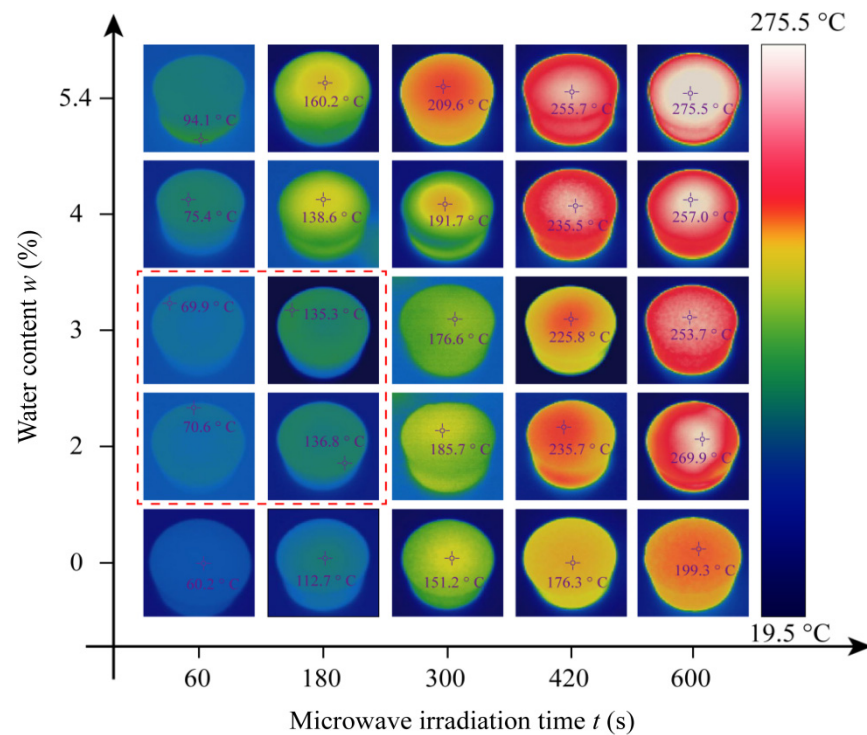


Figure 8. Surface temperature of the sandstone samples for different duration of microwave radiation.

The thermal imaging analysis software IVMS-4800 was used to analyze the variation of surface temperature quantitatively. Eleven temperature measurement points are selected at equal intervals (about 5 mm) along the diameter at the end face of the disc samples, and the arithmetic mean surface temperature of the samples with different water content and duration of microwave radiation is calculated, as shown in Figure 9a. When samples are exposed to a microwave field, the moisture inside the sandstone continuously migrates to the sample's surface and evaporates. The loss of moisture leads to a decrease of the dielectric constants, and the change in dielectric properties will, in turn, affect the microwave heating effect. The relationship between sandstone weight and duration of microwave radiation is shown in Figure 9b. With increasing duration of microwave radiation, the surface temperature of the sample continues to rise, while the corresponding sample weight decreases. The two sets of curves (see Figure 9) can be separated into three stages by using 120 s and 360 s as demarcation points.

In the first stage (0–120 s), for dry sandstone samples, the surface temperature rises slowly due to the low microwave sensitivity. After 120 s of microwave radiation, the average temperature of the dried sample is still below 100 °C, corresponding to a microwave heating rate of less than 0.83 °C/s. With the increase of the initial water content, the temperature rising rate gradually increases. When the water content reaches 5.4%, the average temperature of the sandstone after 120 s of microwave radiation reaches 138 °C, and the corresponding heating rate is about 1.15 °C/s. With the continuous increase of sample temperature, the water evaporation rate also increases, which results for samples with higher water content in a faster mass loss rate.

In the second stage (120–360 s), the surface temperature of the sample generally rises above 100 °C. High temperature accelerates the evaporation and heat dissipation rate of

pore water, and the microwave heat conversion capacity of sandstone is gradually reduced due to the water loss. At the same time, the increasing surface temperature strengthens the convective heat transfer rate with the surrounding air, which ultimately leads to a decrease in the temperature rise rate at this stage. On the other hand, due to the large amount of water vapor released from the rock surface, the weight of sandstone is rapidly decreasing. For dry sandstone samples, because there is no negative heat source from water evaporation, the temperature behavior is the same as in the first stage. However, the weight shows a slight decrease, which may be caused by the loss of some bound water inside the rock.

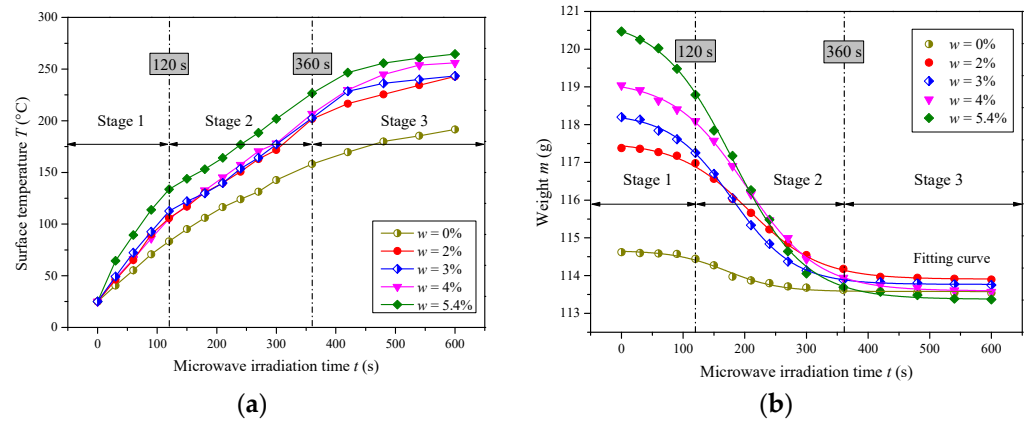


Figure 9. Surface temperature (a) and weight (b) of sandstone vs. microwave irradiation time.

In the third stage (360–600 s), the sandstone is thoroughly dried under continuous microwave irradiation. The evaporation of water inside the sample stagnates, resulting in a constant weight of the sample. At this stage, the main microwave absorbing medium is the rock matrix, not the water inside the sample. Therefore, the thermal conversion efficiency of microwave energy is reduced, and the temperature rising rate of the sample becomes very slow.

Figure 10 shows the microwave heating curves of sandstone under dry and water-saturated conditions, comparing the results from sandstone with results from Zhao et al. [36] and Peinsitt et al. [34]. It is indicated that experimental results are very consistent with those of Zhao et al. and Peinsitt et al. Although there are differences in microwave power, the heating rate of water-saturated sandstone is significantly higher than that of dry samples. In addition, with the increase in microwave power, the effect of water on the microwave heating rate of sandstone is more significant.

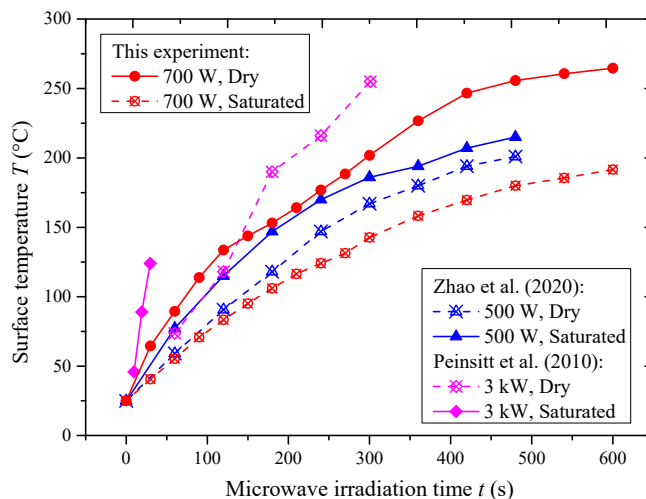


Figure 10. Microwave heating curves of sandstone under dry and water-saturated conditions [34,36].

3.1.2. Porosity and Pore Size Distribution

The nuclear magnetic resonance (NMR) method is adopted to study the pore structure characteristics of sandstone samples before and after microwave radiation. This method is based on the magnetic properties of the atomic nucleus and its interaction with the external magnetic field. The pore distribution of the rock is indirectly obtained by detecting the movement of the hydrogen nucleus inside the water-saturated rock [52,53]. When water-saturated sandstone is placed in a constant magnetic field, applying a radio frequency (RF) electric field will cause hydrogen nuclei to resonate and absorb pulse energy. When the RF field is removed, the absorbed RF energy will be released by the hydrogen nuclei. The process of the H nucleus changing from a high-energy state to a low-energy state is called relaxation, and T_1 and T_2 are the longitudinal and transverse relaxation times, respectively. Since the test results of T_1 and T_2 are basically the same, and T_1 requires more time to measure, the T_2 curve is usually used to characterize the pore distribution characteristics of the rock. Studies have proved that the pore size distribution of the rock is related to the shape and position of the T_2 spectrum. The larger the pore size of the rock, the longer the corresponding relaxation time, and the closer the T_2 distribution curve to the right side of the coordinate axis. Amplitude and peak area of the T_2 curve represent the number of pores in the rock, while the continuity of the curve reflects the connectivity of the pores [54].

Figure 11 shows typical T_2 distribution curves of sandstone with different water content before and after microwave radiation. The T_2 spectrum of the original sandstone sample without microwave irradiation contains three independent amplitudes (P1 is the highest, P2 is the intermediate, and P3 is the lowest), indicating that the sandstone has a wide pore size distribution (more small and medium size pores and fewer large pores). After the dry sandstone experienced microwave radiation, the position of the three peak amplitudes did not change. In contrast, the amplitude of P1 increased slightly, P2 decreased, and the peak value of P3 hardly changed (see Figure 11a). The main reason for this phenomenon may be that the temperature of the sample rises under microwave irradiation, and the thermal expansion of mineral particles causes compaction of medium size pores. As the initial water content of the sample increases, after microwave radiation the amplitudes of the T_2 spectrum continuously shifts towards a larger lateral relaxation time (corresponding to larger pores). The amplitude of P1 decreases while the amplitudes of P2 and P3 increase, indicating that microwave radiation causes the micropores to expand, rupture, and finally merge into larger pores. At the same time, the valleys of the T_2 spectrum gradually rise, which indicates that the connectivity between pores has been enhanced, as shown in Figure 11b,c.

When the initial water content of the sample continually increases to 4%, the P1 amplitude continues to decrease, and the P2 amplitude increases significantly, the originally separated local maxima P2 and P3 gradually merge, which means that the increase in initial water content is conducive for the connectivity of pores. In addition, when the initial water content of the sample exceeds 4%, the P2 amplitude of the T_2 spectrum exceeds the P1 amplitude, indicating that the pore structure has changed, and the average pore size of the sample has increased compared with that before microwave radiation.

According to the pore accumulation curve obtained by the T_2 spectrum, a relationship between the porosity of the microwave irradiated sandstone and its initial water content is obtained, as shown in Figure 12. With increasing initial water content, the porosity of the microwave irradiated sandstone increases exponentially, and according to the different growth rates of the curve, the variation can be divided into two different stages.

In the first stage, the initial water content of sandstone is below 3%. As the initial water content of the sample increases, the porosity of the sandstone after microwave irradiation increases slowly, which may be due to the fact that the samples are soaked in the water for a short time, so that moisture is mainly distributed in the larger pores or natural fissures on the surface of the sample. During microwave radiation, the pore water has strong fluidity, and the generated vapor can easily escape. Therefore, the expansion pressure generated by

the steam in the pores is very limited. On the other hand, the low water content corresponds to a low microwave heating capacity, which results in very limited damage.

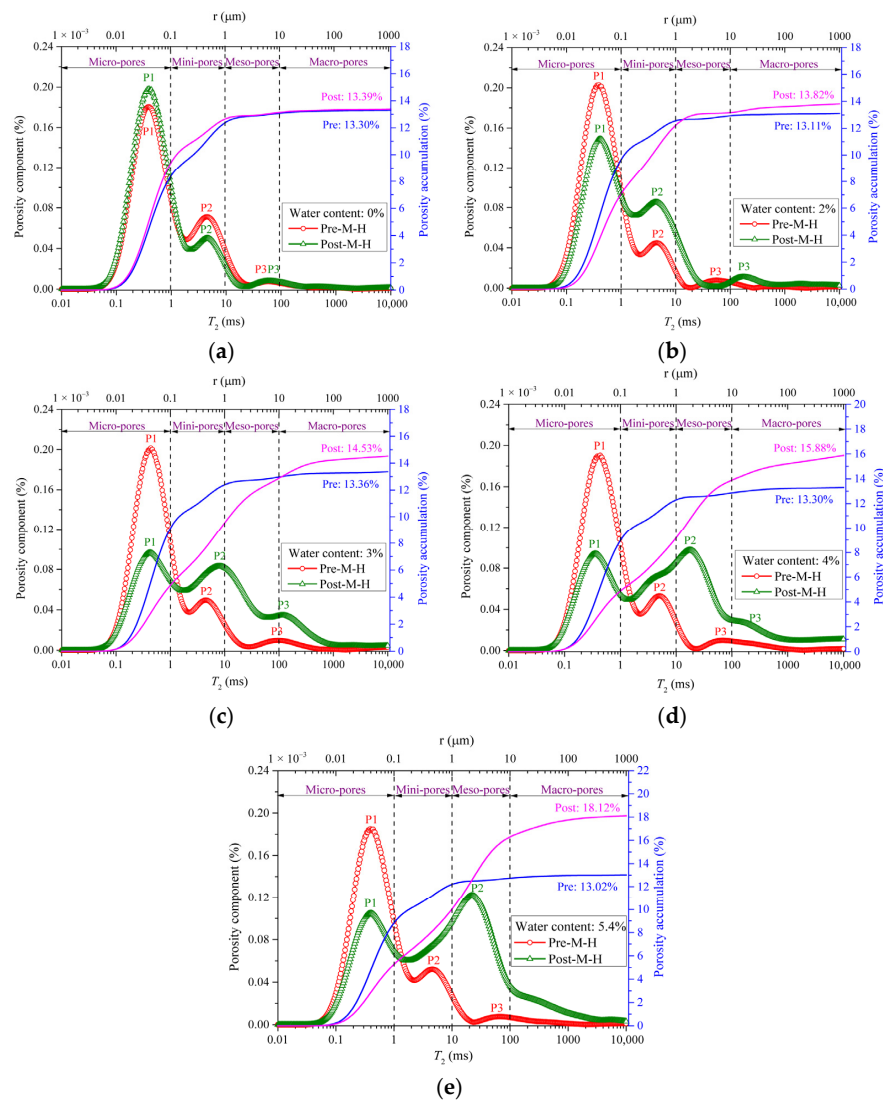


Figure 11. T_2 spectrum: pore size distribution and porosity accumulation curves of the sandstone samples. (a) $w = 0\%$, (b) $w = 2\%$, (c) $w = 3\%$, (d) $w = 4\%$, (e) $w = 5.4\%$.

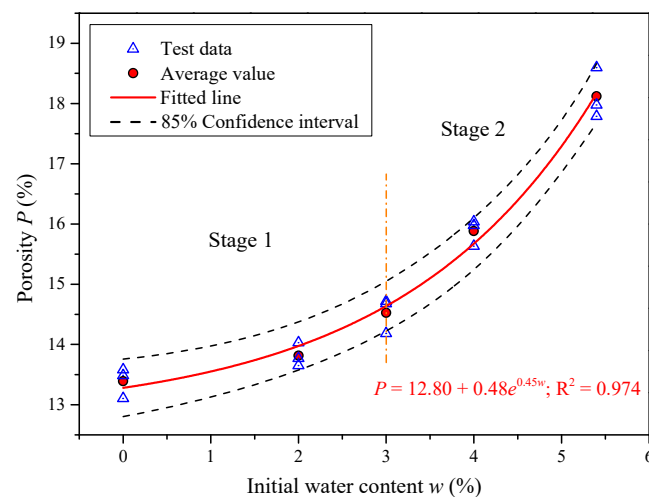


Figure 12. Porosity evolution of microwave irradiated sandstone with different water content.

In the second stage, when the initial water content exceeds 3% and increases to 4% and 5.4%, sufficient immersion time allows water to penetrate the interior of the sample, the dielectric constant of the sandstone rises rapidly, and the microwave heating capacity is also enhanced. Since the rock matrix restricts the evaporation of pore water, a large amount of vapor produces a higher steam pressure in the pores. In addition, as the temperature increases, due to the different thermal expansion coefficients of the different minerals the deformation of the rock increases, resulting in an increase in the microscopic thermal stresses inside the sandstone. Under the combined effect of steam pressure and thermal stress, the initiation and propagation of cracks are intensified, resulting in a significant increase in sandstone porosity after microwave radiation. Therefore, we can conclude that about 3% water content is the critical value (lower limit) that causes the sandstone porosity to increase significantly under microwave radiation. This is consistent with the empirical model of microwave heating proposed by Metaxas and Meredith [55]. By using OriginPro software, the best-fitting formula for porosity and initial water content of sandstone can be expressed as:

$$P = 12.80 + 0.48e^{0.45w}; \quad R^2 = 0.974 \quad (7)$$

where, P is the porosity of the sandstone after microwave radiation, and w is the initial water content of the sample, %.

Rostasy et al. [56] believe that the damage process of rock is a process in which the volume of large pores increases while the volume of small pores decreases. Therefore, studying the variation of sandstone pore diameter under microwave radiation is of great significance for establishing a relationship between water content and sandstone damage evolution. If rock pores are considered simplified as columnar or spherical, then the transverse relaxation time T_2 has the following relationship with the pore radius [57]:

$$\frac{1}{T_2} \approx \rho_2 \left(\frac{F_s}{r} \right)_{pore} \quad (8)$$

where, F_s is the geometrical shape factor, and r is the pore radius, mm. According to Equation (8) the T_2 spectrum relaxation time is proportional to the pore radius, and the T_2 distribution can be transformed into a pore size distribution. According to the division method for pore size proposed by Li et al. [58], this paper divides the sandstone pores into the following four types: micro-pores (<0.1 μm), mini-pores (0.1–1 μm), meso-pores (1–10 μm), and macro-pores (>10 μm).

Figure 13 shows the pore size distribution of sandstone after microwave radiation for different initial water content. There are many micro-pores and mini-pores in the virgin sandstone samples, which account for more than 90% of the total pore volume. At the same time, the number of meso-pores and macro-pores is small, accounting for less than 10% by volume, which indicates that the sandstone used in this paper is relatively tight. When the dry sandstone sample is subjected to microwave radiation, the number of mini-pores and meso-pores increases, while the number of macro-pores and micro-pores decreases, which is related to the compaction of the pores in the rock caused by the thermal expansion of mineral particles [59]. In addition, as the initial water content of the sample increases, the volume ratio of micro-pores after microwave radiation continues to decrease. At the same time, the volume of the other three types of pores increases; that is, the pore size distribution of sandstone shows a trend that the number of large pores increases while the number of small pores decreases, which also indicates that the damage caused by microwave to sandstone increases with the increase of initial water content.

3.1.3. Ultrasonic Features and Damage Factor

In this paper, the HS-YS4A rock acoustic wave parameter tester is adopted to measure the P-wave velocity of the sandstone samples before and after the microwave treatment to quantify the damage caused by the microwave radiation to the rock. During the test, the ultrasonic transducer is aligned with the center of the two ends of the disc sample,

and petroleum jelly is used as a coupling agent to maintain a good coupling between the transducer and the tested sandstone surface. The average value of the P-wave velocity of the dry sandstone samples before microwave treatment was about 2521.3 m/s. After 10 min of microwave radiation, the P-wave velocity was reduced by 3.6%. The decrease of the P-wave velocity indicates that the internal structure has changed, which may be related to the loss of a small amount of bound water inside the rock and the increase of porosity.

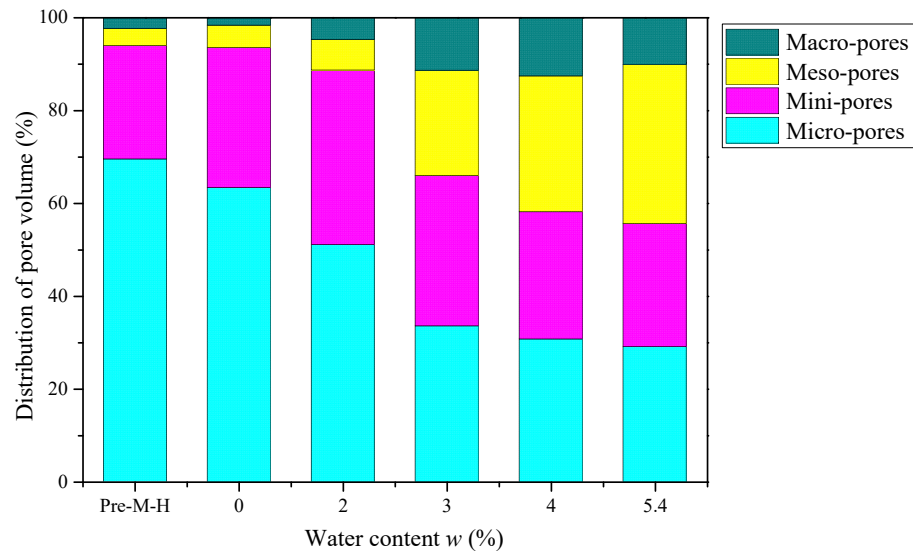


Figure 13. Pore size distribution of sandstone after microwave radiation vs. initial water content.

Figure 14 presents the variations in the P-wave velocity of sandstone under the conditions of different initial water content after microwave radiation. Under the same microwave radiation conditions, when the initial water content of sandstone is 2%, 3%, 4%, and 5.4%, the average P-wave velocity drops by 6.1%, 9.8%, 16.4%, and 30.2%, respectively. The reduction of P-wave velocity is positively correlated with the initial water content of sandstone. The main reason for this phenomenon is that the increase in water content enhances sandstone’s microwave heat conversion efficiency. With the increase of temperature, the pore water evaporates rapidly, and the generated steam pressure leads to an increasing number and size of cracks inside the rock, which finally reduces the propagation speed of ultrasonic waves.

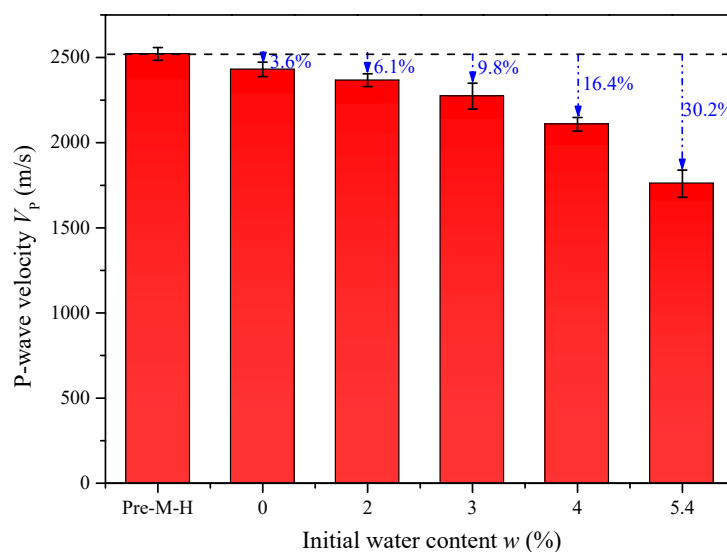


Figure 14. P-wave velocity of sandstone samples vs. initial water content before and after microwave treatment.

It is generally believed that rock strength, Young’s modulus, and ultrasonic wave velocity have a positive correlation, which many test results have confirmed [60]. Microwave radiation changes the internal structure of rocks, and subsequently the strength and deformation characteristics. Because ultrasonic testing is convenient and non-destructive, the relationship between the P-wave velocity and the rock damage characteristics has been extensively studied. The relative variation of P-wave velocity before and after microwave radiation can be used to define a damage factor [61]:

$$D_m = 1 - \left(\frac{V_p}{V_0} \right)^2 \tag{9}$$

where, D_m is the damage factor of the sandstone after microwave radiation, V_0 and V_p represent the P-wave velocity before and after microwave radiation, m/s. In Formula (9), it is stipulated that the damage of sandstone without microwave radiation is 0, and the damage value is 1 when there is a transverse fracture or complete failure in the rock.

The relationship between the damage factor and the initial water content after microwave radiation of the sandstone is shown in Figure 15. With the increase of initial water content, the damage factor of the microwave irradiated sandstone shows a similar growth trend as the porosity (shown in Figure 12). Additionally, taking the initial water content of 3% as the dividing point, the damage evolution can also be divided into two stages: in the first stage (water content is below 3%), the damage value increases from 0.07 to 0.19, and the growth rate is relatively slow. In the second stage (initial water content of sandstone is above 3%), the damage value increases rapidly up to 0.51. The two-stage evolution process of the sandstone damage factor indicates that for microwave-insensitive sandstone, as long as the initial water content of the sample exceeds a specific value, microwave radiation can cause significant damage to the rock. This result can provide an effective solution for the application of microwave fracturing technology in microwave-insensitive rocks. By regression analysis using OriginPro software, damage factor and initial water content are related by the following equation:

$$D_m = 0.015 + 0.048e^{0.433w}; \quad R^2 = 0.988 \tag{10}$$

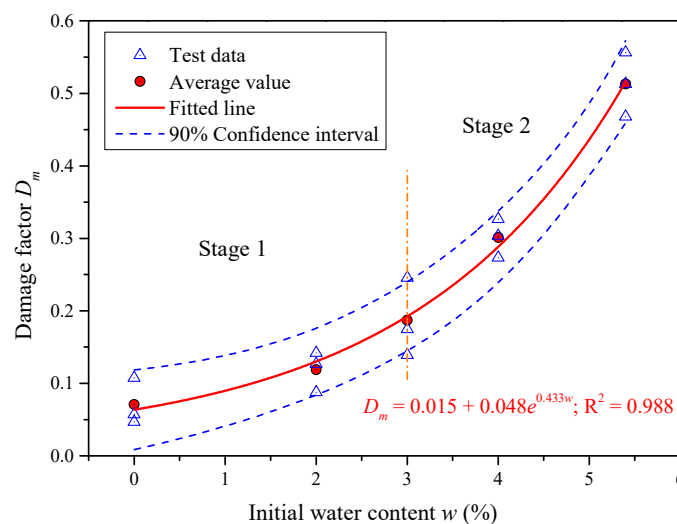


Figure 15. Damage factor vs. initial water content for microwave irradiated sandstone.

3.1.4. Microstructural Observations

The development of pore structure and micro-fractures of sandstone samples before and after microwave radiation were studied using a scanning electron microscope (SEM), as shown in Figure 16. The virgin sandstone samples without microwave radiation show: the rock structure is dense, the mineral surfaces are smooth, and the cementation between min-

eral particles is intact. Some initial pores are observed on the SEM image, but few apparent cracks were found, as shown in Figure 16a. For dry sandstone samples after microwave radiation, the structural roughness and number of pores in sandstone increased, the cementation between mineral particles became loose, and even some narrow intergranular cracks were detected (see Figure 16b).

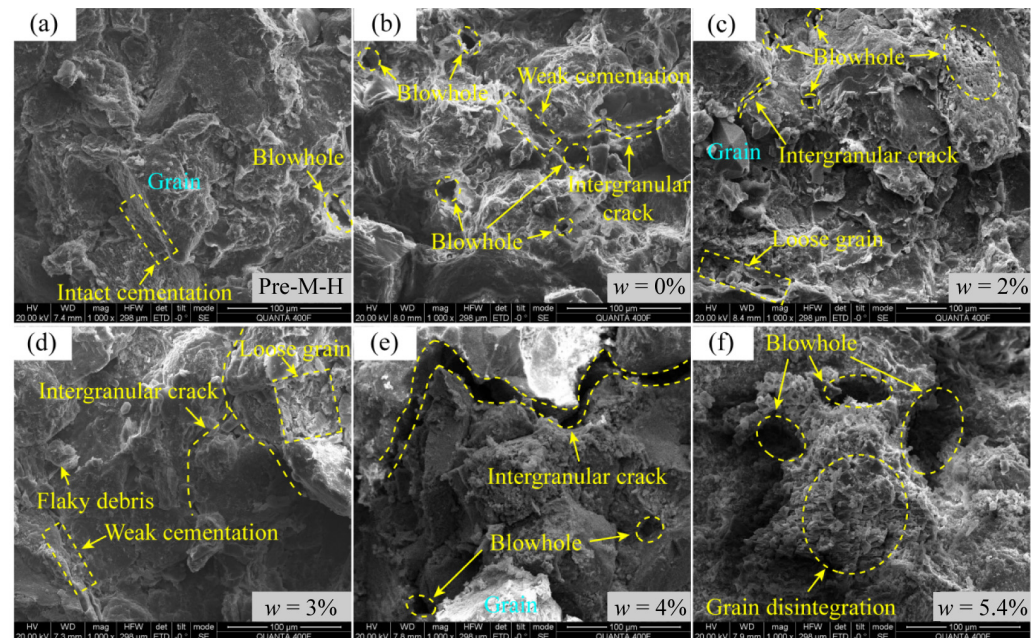


Figure 16. SEM observations of microwave irradiated sandstone with different initial water content. (a) Pre-M-H, (b) $w = 0\%$, (c) $w = 2\%$, (d) $w = 3\%$, (e) $w = 4\%$, (f) $w = 5.4\%$.

As the initial water content of the sample increases, after microwave radiation the connection between the mineral particles of the sandstone is broken, and the number of cracks in the sample increases. At the same time, many loose particles and flaky debris can be found on the sample's SEM image (see Figure 16c,d), which may be due to the rapid evaporation of pore water, causing some pores to disintegrate under gas erosion. When the moisture content reaches 4%, the cementation strength between sandstone particles continues to decrease after microwave radiation, and there are obvious cracks between mineral particles (see Figure 16e). The initiation and propagation of these fractures result in a significant decline in the physical and mechanical properties of the sandstone. When the sandstone is fully saturated (water content is approximately equal to 5.4%), the dielectric loss of the sandstone increases, and the heat energy conversion efficiency is significantly improved. Under the combined effect of thermal stress and steam pressure, internal pores and fissures develop, and ongoing structural collapse occurs (Figure 16f).

3.2. Strength Behavior of Microwave Damaged Sandstone

3.2.1. Quasi-Static Tensile Strength

Figure 17 presents the load–displacement curves of Brazilian tests with sandstone samples with different initial water content after microwave irradiation. It is evident that the deformation processes of all sandstone samples is characterized by three similar phases: (1) micro-crack and pore compaction phase; (2) nearly linear elastic deformation phase; (3) post-failure phase, where the sample loses its bearing capacity immediately after reaching the peak load. The residual stress drops to zero rapidly, which is a typical feature of brittle material failure [62]. Figure 17 shows that with the increase of initial water content, the micro-crack compaction phase of the load–displacement curve extends, the slope of the elastic deformation phase decreases, and the displacement corresponding to the peak load increases. The above phenomena indicate that under microwave radiation, the increase of

initial water content will promote the initiation and propagation of micro-cracks in the rock and weaken the strength and elastic deformation ability.

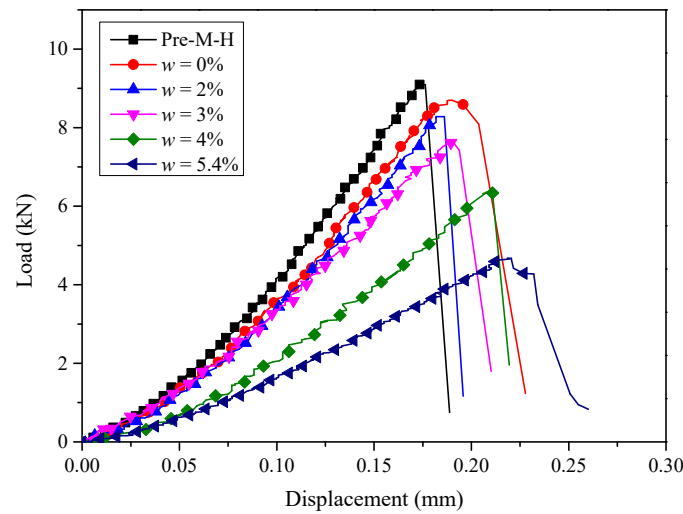


Figure 17. Static Brazilian tests: load–displacement curves of sandstone with different initial water content after microwave irradiation.

According to Equation (3), the quasi-static tensile strength of sandstone was calculated, as shown in Figure 18. For dry sandstone samples, the average value of quasi-static tensile strength before and after microwave treatment is 4.65 and 4.44 MPa, respectively, and the decrease is less than 5%, indicating that the strength weakening effect of microwave radiation on dry sandstone is very limited, which is related to the low microwave sensitivity of dry sandstone. However, it is worth noting that with the increase of the initial water content, the tensile strength of the sandstone significantly decreases after microwave radiation. When the initial water content was 2%, 3%, 4%, and 5.4%, the tensile strength of sandstone after microwave radiation decreased by 9.2%, 16.7%, 30.6%, and 48.9%, respectively.

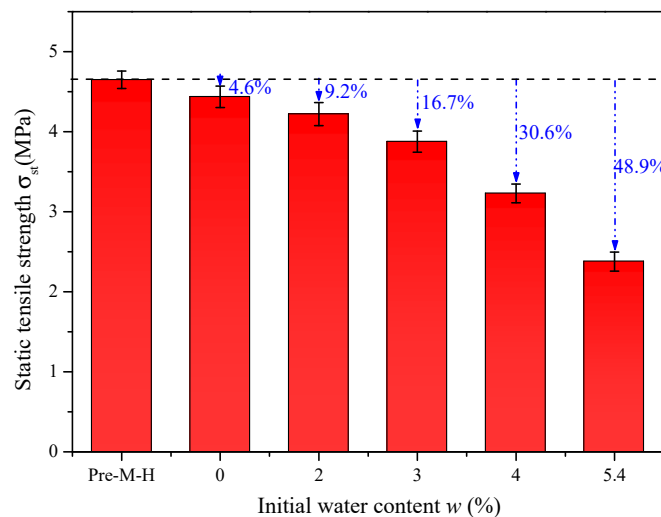


Figure 18. Static Brazilian tests: tensile strength of sandstone with different initial water content after microwave radiation.

Figure 19 shows the relationship between tensile strength and porosity of the microwave irradiated sandstone. The results indicate that as the porosity of sandstone increases, the tensile strength decreases linearly (linear correlation coefficient 0.97). According to our analysis in Section 3.1.2, the increase in sandstone porosity mainly results from the combined effect of thermal damage and steam pressure. Therefore, it is reasonable to

believe that as a strongly polar molecule, water acts as a microwave absorbent and rock fracturing fluid during the microwave radiation of rocks with low dielectric properties. The pore water inside the rock converts microwave energy into heat energy and transfers it to the rock matrix, causing significant thermal damage to the rock. At the same time, the evaporation of water will generate expansion pressure on the original cracks/pores, promote the generation and expansion of cracks and increase the porosity of the sample, and finally results in the continuous reduction of the tensile strength of the rock.

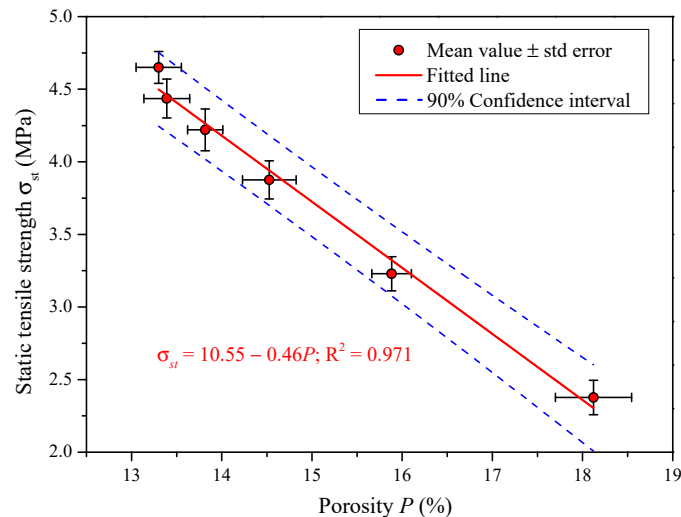


Figure 19. Static tensile strength of microwave irradiated sandstone vs. porosity.

3.2.2. Dynamic Tensile Behavior

Figure 20a shows the typical tensile strength-time curve of microwave irradiated sandstone under impact loading. Different from the static Brazilian tests, after the elastic deformation phase, there is a short plastification phase (large plastic deformation under a high loading rate). In addition, after reaching the peak value, the residual stress level does not disappear suddenly but decreases slowly. The main reason for this phenomenon is that the elastic bar continuously compresses the sample in the post-failure stage.

The initiation and propagation of surface cracks on BD samples were monitored and recorded by a high-speed camera. The camera is connected to the super dynamic strain gauge and triggered by the incident wave to ensure that the recording process is consistent with the stress growth process of the sample. Figure 20a documents that the disc sample maintains its initial integrity during the micro-crack compaction and elastic deformation phase, and there are no apparent cracks visible to the naked eye on the sample surface. When the tensile stress curve reaches the peak point, one tensile crack is generated from the center of the sample and extends to both sides of the sample along the loading direction. With the increase of loading time, secondary tensile cracks were generated near the central crack, and some radial shear cracks at the contact of the disc and the elastic bar began to appear. When the sample is in the post-failure phase, secondary tensile cracks merge with the central crack. At the same time, the wedge-shaped shear cracks are generated at both ends of the sample and expand gradually towards the center of the sample. Finally, they merged with the main crack to form a shear fracture zone parallel to the loading direction.

Figure 20b shows quasi-static and dynamic tensile strength of the samples with different initial water content after microwave irradiation. The dynamic tensile strength is significantly greater than the quasi-static tensile strength, and the tensile strength continues to increase with the increase of the loading rate, showing an apparent loading rate dependence. Under similar loading rate conditions, the dynamic tensile strength of microwave-damaged sandstone decreases with increasing initial water content. The dry sandstone has the highest tensile strength, while the saturated sample has the lowest tensile strength.

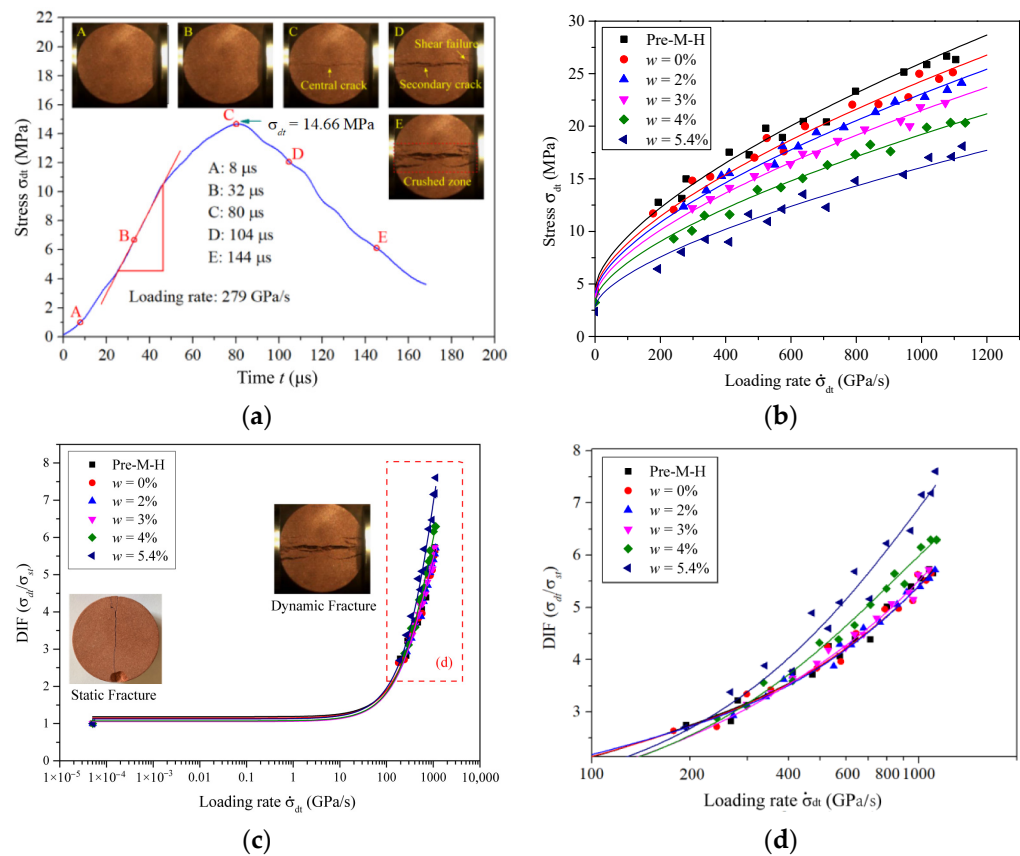


Figure 20. Dynamic Brazilian test results: (a) typical stress-time curve of sandstone sample under impact loading; (b) dynamic tensile strength of the samples under different loading rates; (c) relation between dynamic increase factor and loading rate; (d) magnification of view (c).

As mentioned above, the quasi-static and dynamic tensile strength of sandstone under microwave radiation are mainly influenced by the water content and loading rate. Therefore, it is necessary to propose an empirical formula to comprehensively predict the tensile strength of sandstone under the coupled effect of water content and loading rates. The empirical model equation is introduced as follow in this study:

$$\sigma_{dt} = \sigma_{st}(1 + aw^b)(1 + c\dot{\sigma}_{dt}^d) \tag{11}$$

$$\sigma_{st} = \sigma_{st}^*(1 - \alpha D_m) \tag{12}$$

where σ_{st} and σ_{dt} are, respectively the quasi-static and dynamic tensile strength, MPa; σ_{st}^* is the quasi-static tensile strength without microwave treatment, MPa; w is the initial water content of the sample, %; $\dot{\sigma}_{dt}$ is the loading rates of dynamic BD tests, GPa/s; a , b , c and d are fitting parameters.

It is noteworthy that the thermally induced damage to sandstone caused by microwave radiation can be divided into two parts. The first is the damage caused by thermally induced microcracks and pore expansion. The parameter D_m is defined to describe the first part of damage and can be calculated by using the P-wave velocity. In addition, it is well known that there are many cracks in the sandstone, and thermal deformation can improve the contact state of particles near the cracks. After cooling down, it will not disappear quickly due to plastic deformation and friction. Although the P-wave velocity is significantly reduced due to microwave radiation, the strength of the rock mainly depends on the bearing characteristics of the weakest fracture surface. The improved contact state between mineral particles due to thermal deformation cannot be detected by the P-wave velocity. Hence, this study uses the damage correction parameter α to describe the second damage, and the value of α would be generally less than 1, which can be determined by fitting the

quasi-static tensile strength data. The fitting curves of the dynamic tensile strength are given in Figure 20b and indicate that the empirical formula provides a good prediction for the data points, where $\alpha = 0.95$, $a = 8.7063 \times 10^{-6}$, $b = 5.9761$, $c = 0.054$ and $d = 0.6433$. The R-square of Equations (11) and (12) in this study are, respectively 0.984 and 0.994.

To quantify the effect of loading rate on the tensile strength of sandstone, the ratio of dynamic tensile strength to quasi-static tensile strength is defined as the dynamic increase factor (DIF), as shown in Figure 20c,d. The value of DIF increases significantly with the increase of loading rate, and the dynamic tensile strength of sandstone with different water content can be increased by more than 6 times after microwave radiation. The inherent defects in rock materials (including pores, grain boundary cracks, etc.) exhibit different characteristics under different loading rates. Under static load of a certain level crack coalescence happens and macroscopic fractures can be formed, whereas at the same load level due to the short impact of the load crack coalescence is limited in case of dynamic loading conditions, as already discussed by Rubin and Ahren [63], Zhao and Li [64].

An interesting phenomenon can be found in Figure 20d: when the initial water content of the sandstone is within 3%, the DIF curves basically coincide, but when the initial water content exceeds 3%, the DIF curves deviate, which indicates that sandstone with high water content can exhibit higher sensitivity to loading rate after being subjected to microwave radiation. The main reason for this phenomenon is that the crack density of sandstone with high initial water content increases significantly after microwave radiation. Similar conclusions were also drawn in the study by Wu et al. [65] on rock's dynamic loading rate dependence under pre-stressed loading conditions. They believe that the increase of activated cracks makes the rock a more viscous material. At the same loading rate, rocks with greater viscosity show higher loading rate sensitivity.

3.2.3. Energy Dissipation

Energy dissipation is the driving force of material destruction, reflecting the continuous evolution of internal cracks/defects in the material and the continuous weakening and loss of overall strength. Rock crushing is usually a process of converting mechanical energy into rock crushing energy [66,67]. Under the action of impact loading, energy is transferred in the form of stress waves. According to the elastic wave theory, the energy carried by each waveform in the SHPB system can be calculated according to the following formula [28]:

$$W_I = E_e A_e C_e \int_0^\tau \varepsilon_I(t)^2 dt \quad (13)$$

$$W_R = E_e A_e C_e \int_0^\tau \varepsilon_R(t)^2 dt \quad (14)$$

$$W_T = E_e A_e C_e \int_0^\tau \varepsilon_T(t)^2 dt \quad (15)$$

where, W_I , W_R , and W_T represent the energy carried by the incident wave, reflected wave and transmitted wave, J ; C_e is the longitudinal wave velocity of the elastic bar (5400 m/s), and τ is the moment when the sample is completely destroyed. According to the law of conservation of energy, if the energy lost by the friction between the elastic bar and the sample is neglected, the energy absorbed by the sample can be expressed as [28]:

$$W_S = W_I - W_R - W_T \quad (16)$$

Figure 21a shows typical energy-time curves of sandstone obtained from dynamic Brazilian tests. It can be found that with the extension of the loading time, each energy curve shows a similar "S-shaped" growth, and all energies firstly increase to a specific value and then remain stable. The relationship between the magnitude of each energy type is: incident energy > reflection energy > absorption energy > transmission energy. In the dynamic Brazilian tests, the incident wave propagates along the elastic bar towards the sample. Because the contact area between the disc sample and the elastic bar is small, a

large portion of the energy is reflected, the sample absorbs part of the energy, and only a small amount of energy can be transferred to the transmission bar through the sample, which results in the smallest transmission energy of all energies. The absorbed energy of the sample mainly includes the energy absorbed by crack propagation and failure of the sample as well as the kinetic energy of the fragments flying away. The existing studies have shown that the energy used for crack propagation and failure of the sample accounts for more than 95% of the total absorbed energy. Therefore, in our research, the kinetic energy of the flying fragments is ignored, and the sample absorption energy is used to replace the crushing energy consumption.

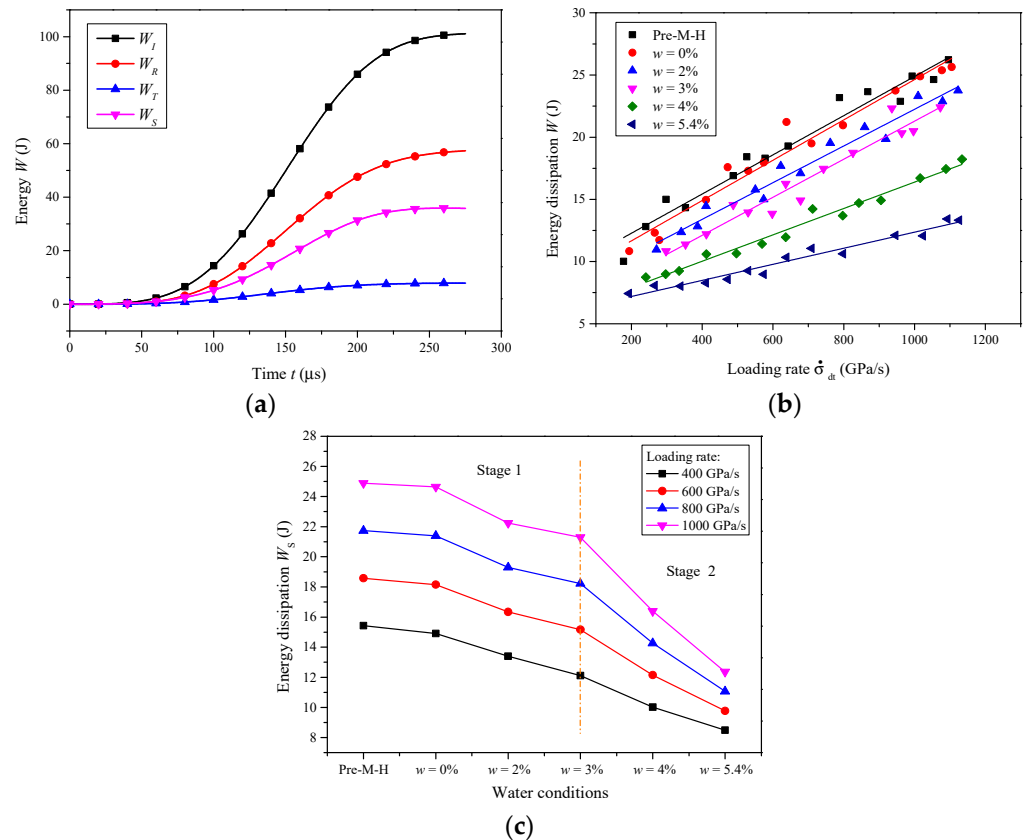


Figure 21. Energy analysis of sandstone after microwave irradiation: (a) typical energy-time curve of sample under dynamic loading; (b) energy dissipation vs. loading rate; (c) energy dissipation vs. water content.

Figure 21b shows the energy dissipation curves of the sandstone samples from the dynamic splitting tensile tests. It can be found that the energy dissipation of sandstone with different water content increases obviously with the increase of loading rate. This phenomenon may be related to the fact that the initial cracks in the rock cannot propagate and aggregate along the direction with the lowest energy consumption under fast loading. A linear fitting can express the relation between dissipated energy and loading rate:

$$\begin{cases} W_{S(\text{Pre-M-H})} = 9.12 + 0.0158\dot{\sigma}_{dt}; R^2 = 0.919 \\ W_{S(w=0\%)} = 8.42 + 0.0163\dot{\sigma}_{dt}; R^2 = 0.926 \\ W_{S(w=2\%)} = 7.49 + 0.0148\dot{\sigma}_{dt}; R^2 = 0.935 \\ W_{S(w=3\%)} = 5.99 + 0.0153\dot{\sigma}_{dt}; R^2 = 0.894 \\ W_{S(w=4\%)} = 5.78 + 0.0106\dot{\sigma}_{dt}; R^2 = 0.959 \\ W_{S(w=5.4\%)} = 5.90 + 0.0065\dot{\sigma}_{dt}; R^2 = 0.921 \end{cases} \quad (17)$$

During the test, loading with different strain rate was achieved by adjusting the impact air pressure and the striker's position in the launch tube. However, small changes in the size of the rock sample and the loading air pressure affects the strain rate of the sample. We use the fitting formula obtained by Equation (17) to calculate the relationship between the energy dissipation of the sandstone and the initial water content under the specified loading rate, as shown in Figure 21c. Under a given loading rate, the energy dissipation gradually decreases with the increase of the initial water content of the rock. The main reason is that the presence of moisture improves the heat transfer capacity of sandstone under microwave radiation. The effect of high temperature weakens the bonds between crystal particles and increases the crack density. Under dynamic loading conditions, cracks and pores appear by absorbing mechanical energy. However, after microwave radiation the required energy for rock fragmentation is reduced. In addition, when the initial water content of sandstone exceeds 3% (the corresponding water saturation is about 55.6%), the decline rate of the energy dissipation curve increases significantly, which is related to the increase in vapor pressure generated by the evaporation of pore water inside the rock. The above analysis shows that the existence of water under the effect of microwave radiation can aggravate the microwave damage of the rock, and the water saturation of the rock has a critical value of 55.6%. When the water saturation exceeds 55.6%, the pre-splitting failure of rock caused by microwave radiation is intensified, significantly reducing the energy consumption of mechanical rock crushing.

4. Discussion

4.1. Microwave Heating and Cracking Mechanisms

Microwave heating is a process that uses the dielectric properties of materials to convert microwave energy into heat energy. According to the difference in dielectric properties, materials can be divided into three different media: microwave conductors, microwave insulators and microwave absorbers, as shown in Figure 22a. Three different media exhibit different thermal responses under microwave radiation. Microwave conductors can be directly penetrated by microwaves, with no microwave energy loss and no thermal effect on the material, such as glass, ceramics and other non-metallic materials. Microwave insulators totally reflect microwaves, and such materials can be exposed to microwaves for long periods without being heated, such as most metallic materials. Microwave energy can be partially or fully absorbed by microwave absorbers and will be converted into heat; some metallic minerals have a strong microwave absorption capacity, such as hematite, etc. [68]. The sandstone material selected in this paper has relatively low dielectric properties and can be considered as a weak microwave absorber. During the microwave radiation, most of the microwave energy will pass through the sandstone sample, and only a small part of the microwave energy will be absorbed and converted into heat energy. Therefore, as the microwave radiation time increases, the heating rate of the dry sandstone samples is relatively low.

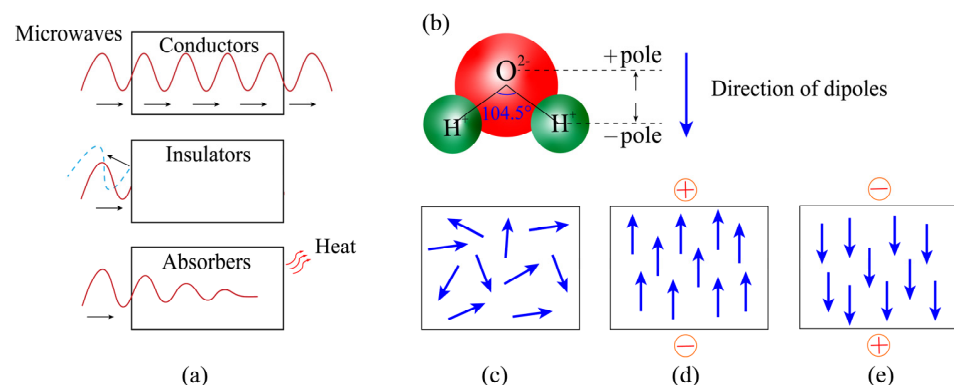


Figure 22. (a) Interaction of microwave with different materials; (b) the structure of water molecule; (c) direction of dipoles under natural state; (d,e) dipoles rotate influenced by electric field.

Although microwaves can easily penetrate the sandstone matrix, polar molecules such as water can absorb microwaves and thus be heated. It can be observed from Figure 22b that the water molecule structure is composed of two hydrogen atoms and one oxygen atom. Since the bond angle of the two H-O bonds of the water molecule is 104.5° , their folded structure leads to the separation of the positive and negative poles, resulting in a dipole [69]. In the natural state, the direction of dipoles is in random order (Figure 22c). However, when placed in a microwave field, the orientation of the dipoles will change as the microwaves alternate, and the adjacent molecules rub and collide with each other, resulting in a violent heating phenomenon. The heat absorbed by the water propagates to the surrounding rock matrix through conduction and convection, increasing the temperature of the water-bearing sandstone, as shown in Figure 9a.

However, as the temperature rises, the water undergoes a phase change towards water vapor. The vapor exerts pressure on the inner wall of the pores and cracks and promotes the formation and development of internal fractures. The microscopic morphological characteristics of sandstone samples can reveal this (see Figure 16). The dielectric properties of rock mass increase due to the presence of moisture, leading to an increase in the microwave thermal conversion capacity and intensify the internal damage of the rock. Therefore, it can be considered that the pore water acts as both: microwave absorber and fracturing fluid during microwave irradiation of sandstone. Figure 23 presents a simplified scheme to illustrate the microwave heating process and damage mechanisms of water-bearing sandstone.

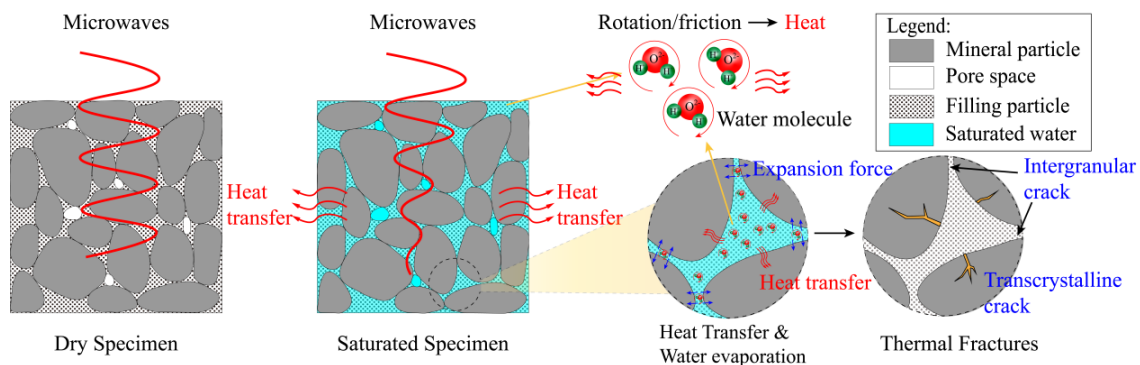


Figure 23. Microwave heating process and damage mechanisms of water-bearing sandstone.

To explain the damage and failure process of rock from a mesoscopic perspective, we assume that there are two basic types of cracks in the rock simultaneously, namely, wing cracks and circular pores, as shown in Figure 24a. For saturated sandstone samples, the wing cracks and pores are filled with free water. Under microwave radiation, water undergoes a phase change and forms water steam. A binary gas mixture composed of water vapor and air is formed inside the cracks and pores. Since the pore size limits the volume expansion of the water molecules, expansion pressure will be generated inside the rock and applied to the inner walls of cracks and pores. For a wing-shaped crack, both sides are subjected to compressive stress, and the maximum tensile stress appears at both ends of the crack. Therefore, when the vapor pressure exceeds the ultimate tensile strength of the pore structure, secondary cracks will begin to form at the tip of the wing crack. The vapor pressure generated by the volume expansion of water molecules is considered uniform for circular pores. Moreover, as the vapor pressure rises, new cracks will be generated symmetrically from any two ends of the circular hole. Due to the lack of suitable pressure sensing equipment and measurement methods, we cannot directly measure the pressure in the pores and cracks. However, the approximate solution for the relationship between saturated vapor pressure and temperature of the rock is given by the following formula [70]:

$$P_{\text{sat}} = 0.61121 \exp \left(\left(18.678 - \frac{T}{234.5} \right) \left(\frac{T}{257.14 + T} \right) \right) \quad (18)$$

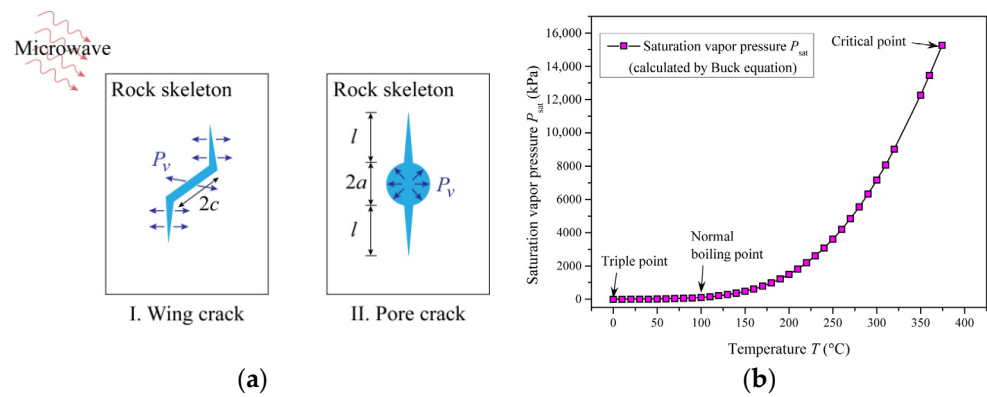


Figure 24. Two types of crack mode (a) and the variation of saturation vapor pressure with increasing temperature (b).

Substituting our test data into Formula (18), the relationship between the saturated vapor pressure and temperature can be obtained, as shown in Figure 24b. The saturated vapor pressure increases exponentially with increasing temperature. When the temperature exceeds the water boiling point (100 °C), the growth rate of the saturated vapor pressure accelerates, which is related to a significant volume expansion of water molecules after reaching the boiling point.

However, in our research, the sandstone samples have different initial water content. As the duration of microwave radiation increases, the water gradually evaporates and escapes, resulting in a continuous decrease in the water content of the samples. Therefore, the vapor pressure inside the rock is a function of moisture content and temperature. According to the research of Gulati et al. [71], under different temperature and water content conditions, the vapor pressure inside the rock cracks/pores can be determined as:

$$P_v = P_{sat} \exp[-0.0267w_t^{-1.656} + 0.0107e^{-1.287w_t} w_t^{-1.513} \ln(P_{sat})] \tag{19}$$

$$w_t = \frac{m_t - m_e}{m_e} \tag{20}$$

where, P_{sat} is the saturated vapor pressure at a certain temperature, MPa; m_t and w_t are, respectively the weight (g) and water content (%) of the sandstone at a certain time of microwave radiation, respectively; m_e represents the weight of sandstone that has been completely dried by the microwave oven, g/. The variations of vapor pressure for five sandstone samples (initial moisture contents of 0%, 2%, 3%, 4%, and 5.4%) versus duration of microwave irradiation are presented in Figure 25. The results show that with the increase of microwave radiation time, the internal vapor pressure of sandstone samples with different water content presents a similar pattern: first increase and then decrease, which is related to the increase of pore water temperature and the continuous decrease of water content. In addition, the maximum vapor pressure inside the rock increases with increasing water content, and the microwave radiation time required to reach the peak value of vapor pressure also gradually increases. This phenomenon indicates that high water content generates high vapor pressure, and the vapor pressure acts over a longer time span. The maximum value of steam pressure generated by all samples exceeds the standard atmospheric pressure, which provides the possibility for crack expansion inside the rock. Moreover, the maximum vapor pressure of the saturated sample is always lower than the quasi-static tensile strength of the sandstone, which also ensured that the water-bearing sandstone will not produce macro cracks and disintegration by applying 700 W microwave radiation.

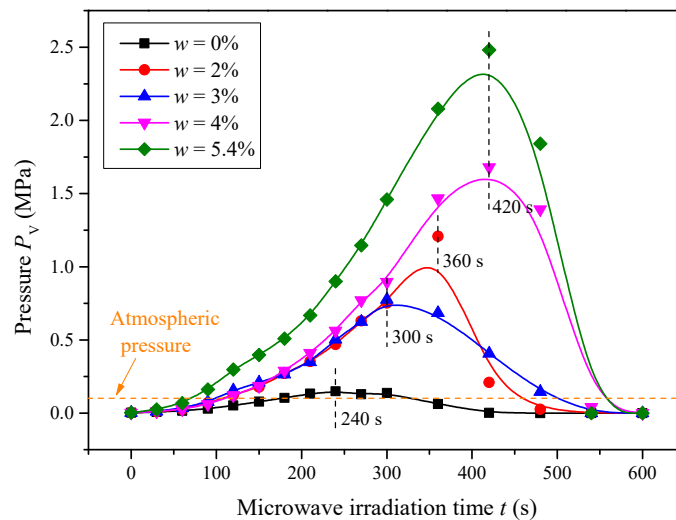


Figure 25. Variation of vapor pressures inside sandstone vs. microwave irradiation time.

Previous studies have shown that the growth of cracks inside the rocks is highly dependent on the development of thermal stresses [72]. Under microwave radiation conditions, due to differences in the dielectric constants, thermal expansion coefficients, and strength of different mineral particles, the mineral particles will generate uneven expansion and deformation. The thermal strain mismatch leads to shear stress generated at the mineral interface. Many intergranular cracks will be generated when the stress exceeds the bonding strength of the particles (see Figure 16). In addition, overheating is likely to occur inside the sample due to the uneven distribution of pore water and the high microwave sensitivity of a few minerals. Under extreme temperatures, the phase transformation and decomposition of different rock-forming minerals are also important reasons for the deterioration of the sandstone. For example, quartz has a phase transition from α quartz to β quartz at $573\text{ }^{\circ}\text{C}$, connected with a drastic volume change [22,73]. The main component of calcite is calcium carbonate, which will undergo a decomposition reaction at about $500\text{ }^{\circ}\text{C}$, and its products are CaO and CO_2 . The expansion pressure generated by CO_2 will also accelerate the damage and crack propagation of the rocks [74,75].

4.2. Industrial Application and Challenges

As discussed above, moisture has a positive effect on microwave induced fracturing of sandstone. The initial water content increases the ability of the rock to absorb microwaves. The combined effect of thermal stress and steam pressure helps the microwaves to induce intergranular cracks in the rock. Due to the overheating effects in the rock, some minerals may undergo a phase transformation reaction, which will also lead to the breakage of the rock structure. Therefore, for the industrial application of microwave technology, we can get the following enlightenment: (1) when excavating microwave-insensitive rock mass, water can be injected into the rock mass to increase the dielectric properties, providing an effective solution for the application of microwave fracturing technology in microwave-insensitive rocks. (2) microwave radiation can increase the density of rock mass fractures when excavating deep brittle rock masses with high in situ stress and high storage of elastic energy. The stored elastic energy of the rock mass near the working face can be released, thereby effectively avoiding a rock burst disaster during mechanical excavating. (3) microwave radiation is helpful to fracture rock layers and improve the porosity and pore connectivity of water-bearing rock masses. During the exploitation of deep underground geothermal resources, microwave radiation has the potential to enhance the permeability of the rock mass and to improve fluid circulation.

Although laboratory tests have indicated that microwave-assisted rock breaking technology has obvious advantages, there are also a series of challenges for practical engineering applications: (1) More microwave energy absorbed by the rock mass is beneficial for in-

creasing the fracture density, but penetration of the microwave will decrease. Therefore, determining the best microwave radiation parameters for each rock mass is worth studying. (2) Microwave radiation can cause severe damage to the human body. Therefore, the equipment has to fulfill certain safety requirements. (3) Microwaves have attenuation and reflection losses when radiating the rock surface, so that microwave energy is not fully applied to the excavated rock mass, reducing the energy utilization rate. Therefore, the economics of microwave-assisted rock-breaking technology needs to be further evaluated.

4.3. Recommendations for Further Work

Up to now, considerable efforts have been made to investigate changes in the physical and mechanical properties of rocks subjected to microwave irradiation. However, the factors that may affect the microwave weakening degree of rocks have not been fully investigated, and relatively little research has been done on introducing microwave heating into engineering applications. Based on the existing studies, some recommendations for future work are outlined.

(1) Most previous studies on the reactions of rocks to microwave radiation have been carried out using multi-mode microwave ovens. Compared with single-mode microwave cavities, multi-mode microwave ovens have the advantages of uniform heating, high energy utilization and no risk of microwave leakage, but the power density is relatively low and only suitable for laboratory tests. Therefore, after fully understanding the damage behavior of microwaves on small-sized rock samples, a high-power single-mode microwave cavity is required to carry out face radiation tests on large-sized rock masses.

(2) In engineering practice, mechanical cutting and microwave irradiation sometimes need to be carried out simultaneously to further enable continuous excavation for underground works and tunneling operations. Therefore, it is still essential to test the dynamic mechanical properties of rocks under microwave heating conditions. Furthermore, how to prevent microwave leakage during impact loading is a problem that needs to be addressed first.

(3) Cutting and drilling tests of microwave-irradiated rocks considering in situ stresses should be carried out, thus facilitating the industrial application of microwave-assisted rock breaking. In addition, if microwave irradiation is carried out simultaneously with mechanical excavation, the effect of high temperatures on the durability of the drill bit or cutter head needs to be further investigated.

(4) Microwave radiation is a multi-field coupled heating process influenced by electromagnetic, temperature, stress and mass transfer fields. It is necessary to perform a finite element or discrete element method analysis of the mechanical behavior of rocks under microwave radiation to determine the relationship between microwave-induced temperature distribution, thermal stress and fracture density.

5. Conclusions

This study documented low-power microwave radiation tests on sandstone samples with different water content. Some essential physical properties of sandstone samples, including surface temperature, porosity, and P-wave velocity, were determined. The influence of water content on the dynamic tensile strength, rate dependence, energy dissipation, and failure mechanisms of sandstone subjected to microwave irradiation was investigated. The following major conclusions can be drawn:

(1) The presence of pore water can significantly improve the heating effect of microwave-insensitive rocks. With the increasing water content, the pore size distribution of sandstone shows a trend that the number of large pores increases while the number of small pores decreases. Especially if the initial water content of the sample exceeds 3%, the physical parameters change significantly with the increase of water content.

(2) For different initial water content, the dynamic tensile strength of microwave-irradiated sandstone increases with increasing loading rate. The higher the initial water content of the sample, the stronger the dependence on the loading rate, which is related to the increasing crack density and the increase in the sample's viscosity.

(3) Under the same loading rate, the energy consumption by fragmentation of the sample decreases with the increase of the moisture content, which indicates that the existence of pore water is beneficial to increase the damage caused by microwave radiation.

(4) The SEM images show that the internal fractures of the sandstone samples after microwave radiation are mainly intergranular cracks, and as the initial water content of the sample increases, the crack density increases. The combined effect of thermal stress and steam pressure supports the microwave to induce intergranular cracks in the rock sample.

Author Contributions: Methodology, P.W.; investigation, P.W. and T.Y.; writing—original draft preparation, P.W.; writing—review and editing, T.Y. and H.K.; project administration, X.L.; funding acquisition, X.L. and T.Y. All authors have read and agreed to the published version of the manuscript.

Funding: This research was funded by the National Natural Science Foundation of China (Nos. 41972283 and 11972378), the National Key Scientific Instrument and Equipment Development Project of China (No. 51927808), and the Hunan Provincial Innovation Foundation for Postgraduates of China (No. CX2018B066).

Data Availability Statement: The data presented in this study are available on request from the corresponding author.

Conflicts of Interest: The authors declared that there are no conflict of interest to the work reported in this paper.

Nomenclature

BD	Brazilian disc
DIF	Dynamic increase factor
ISRM	International Society for Rock Mechanics
MTS	Material test system
NMR	Nuclear magnetic resonance
RF	Radio frequency
SEM	Scanning electron microscope
SHPB	Split Hopkinson pressure bar
a	Fitting parameters
A_e	Cross-sectional area of elastic bars (mm^2)
A_w	Water absorption (%)
B	Thickness of the specimen (mm)
C_p	Primary P-wave velocity (m/s)
D	Diameter of the specimen (mm)
D_m	Damage value of specimen
E_e	Elastic modulus of elastic bars (GPa)
E_s	Elastic modulus in quasi-static tests (GPa)
F_1	Force between the specimen and incident bar (kN)
F_2	Force between the specimen and transmission bar (kN)
F_s	The geometric shape factor of pores in specimen
m_d	Dry weight of the specimen (g)
m_w	Wet weight of the specimen (g)
m_t	Weight of the specimen at a certain time (g)
m_e	Weight of the microwave completely dried specimen (g)
P	Porosity (%)
P_{sat}	The saturated vapor pressure of pure water (MPa)
P_v	The vapor pressure inside the specimen (MPa)
r	The pore radius (mm)
R^2	Coefficient of correlation
t	Water soaking time of the specimen (h)
V_0	P-wave velocity of specimen before microwave irradiation (m/s)
V_p	P-wave velocity of specimen after microwave irradiation (m/s)
W_I	Incident energy (J)
W_R	Reflection energy (J)

W_S	Absorption energy (J)
W_T	Transmission energy (J)
w	Water content of the specimen (%)
w_s	Saturated water content of the specimen (%)
ρ	Density (kg/m ³)
σ_c	Uniaxial compressive strength in quasi-static tests (MPa)
σ_{dt}	Dynamic indirect tensile strength of the specimen (MPa)
σ_{st}	Indirect tensile strength in quasi-static tests (MPa)
σ_{st}^*	Quasi-static tensile strength without microwave treatment (MPa)
ε_I	Signal on the incident bar
ε_R	Signal on the reflected bar
ε_T	Signal on the transmitted bar

References

- Li, X.B.; Yao, J.R.; Du, K. Preliminary study for induced fracture and non-explosive continuous mining in high-geostress hard rock mine—A case study of Kaiyang phosphate mine. *Chin. J. Rock Mech. Eng.* **2013**, *32*, 1101–1111.
- Du, K.; Tao, M.; Li, X.B.; Zhou, J. Experimental study of slabbing and rockburst induced by true-triaxial unloading and local dynamic disturbance. *Rock Mech. Rock Eng.* **2016**, *49*, 3437–3453. [[CrossRef](#)]
- Xia, Y.M.; Zhang, K.; Liu, J.S. Design optimization of TBM disc cutters for different geological conditions. *World J. Eng. Technol.* **2015**, *3*, 218–231. [[CrossRef](#)]
- Rostami, J. Performance prediction of hard rock Tunnel Boring Machines (TBMs) in difficult ground. *Tunn. Undergr. Space Technol.* **2016**, *57*, 173–182. [[CrossRef](#)]
- Ciccu, R.; Grosso, B. Improvement of disc cutter performance by water jet assistance. *Rock Mech. Rock Eng.* **2014**, *47*, 733–744. [[CrossRef](#)]
- Shi, X.M.; Duan, Y.L.; Han, B.; Zhao, J. Enhanced rock breakage by pulsed laser induced cavitation bubbles: Preliminary experimental observations and conclusions. *Geomech. Geophys. Geo.-Energy Geo.-Resour.* **2020**, *6*, 25. [[CrossRef](#)]
- Kocis, I.; Kristofic, T.; Gajdos, M.; Horvath, G.; Jankovic, S. Utilization of electrical plasma for hard rock drilling and casing milling. In Proceedings of the SPE/IADC Drilling Conference and Exhibition, London, UK, 17–19 March 2015.
- Zheng, Y.L.; Zhang, Q.B.; Zhao, J. Challenges and opportunities of using tunnel boring machines in mining. *Tunn. Undergr. Space Technol.* **2016**, *57*, 287–299. [[CrossRef](#)]
- Wang, S.F.; Li, X.B.; Yao, J.R.; Gong, F.Q.; Li, X.; Du, K.; Tao, M.; Huang, L.Q.; Du, S.L. Experimental investigation of rock breakage by a conical pick and its application to non-explosive mechanized mining in deep hard rock. *Int. J. Rock Mech. Min. Sci.* **2019**, *122*, 104063. [[CrossRef](#)]
- Aydin, G.; Karakurt, I.; Aydin, K. Wear performance of saw blades in processing of granitic rocks and development of models for wear estimation. *Rock Mech. Rock Eng.* **2013**, *46*, 1559–1575. [[CrossRef](#)]
- Karakurt, I.; Aydin, G.; Aydin, K. Experimental and statistical analysis of cutting force acting on diamond sawblade in sawing of granitic rocks. *Proc. Inst. Mech. Eng. Part B J. Eng. Manuf.* **2013**, *227*, 286–300. [[CrossRef](#)]
- Wei, W.; Shao, Z.S.; Zhang, Y.Y.; Qiao, R.J.; Gao, J.P. Fundamentals and applications of microwave energy in rock and concrete processing—A review. *Appl. Therm. Eng.* **2019**, *157*, 113751. [[CrossRef](#)]
- Hassani, F.; Nekoovaght, P.M.; Gharib, N. The influence of microwave irradiation on rocks for microwave-assisted underground excavation. *J. Rock Mech. Geotech. Eng.* **2016**, *8*, 1–15. [[CrossRef](#)]
- Nekoovaght, P. An Investigation on the Influence of Microwave Energy on Basic Mechanical Properties of Hard Rocks. Master's Thesis, Concordia University, Montreal, QC, Canada, 2009.
- Ge, Z.L.; Sun, Q. Acoustic emission characteristics of gabbro after microwave heating. *Int. J. Rock Mech. Min. Sci.* **2021**, *138*, 104616. [[CrossRef](#)]
- Lu, G.M.; Feng, X.T.; Li, Y.H.; Zhang, X.W. Influence of microwave treatment on mechanical behaviour of compact basalts under different confining pressures. *J. Rock Mech. Geotech. Eng.* **2020**, *12*, 213–222. [[CrossRef](#)]
- Yang, B.G.; Gao, M.Z.; Xie, J.; Liu, J.J.; Wang, F.; Wang, M.Y.; Wang, X.; Wen, X.Y.; Yang, Z.Y. Exploration of weakening mechanism of uniaxial compressive strength of deep sandstone under microwave irradiation. *J. Cent. South Univ.* **2022**, *29*, 611–623. [[CrossRef](#)]
- Kahraman, S.; Canpolat, A.N.; Fener, M. The influence of microwave treatment on the compressive and tensile strength of igneous rocks. *Int. J. Rock Mech. Min. Sci.* **2020**, *129*, 104303. [[CrossRef](#)]
- Satish, H.; Ouellet, J.; Raghavan, V.; Radziszewski, P. Investigating microwave assisted rock breakage for possible space mining applications. *Min. Technol.* **2006**, *115*, 34–40. [[CrossRef](#)]
- Zheng, Y.L.; Zhang, Q.B.; Zhao, J. Effect of microwave treatment on thermal and ultrasonic properties of gabbro. *Appl. Therm. Eng.* **2017**, *127*, 359–369. [[CrossRef](#)]
- Hartlieb, P.; Kuchar, F.; Moser, P.; Kargl, H.; Restner, U. Reaction of different rock types to low-power (3.2 kW) microwave irradiation in a multimode cavity. *Min. Eng.* **2018**, *118*, 37–51. [[CrossRef](#)]
- Li, Q.; Li, X.; Yin, T. Effect of microwave heating on fracture behavior of granite: An experimental investigation. *Eng. Fract. Mech.* **2021**, *250*, 107758. [[CrossRef](#)]

23. Nejati, H.; Hassani, F.; Radziszewski, P. Experimental investigating of fracture toughness reduction and fracture development in basalt specimens under microwave illumination. In Proceedings of the Earth and Space Conference, Denver, CA, USA, 11–13 April 2012; pp. 325–334.
24. Shepel, T.; Grafe, B.; Hartlieb, P.; Drebenstedt, C.; Malovyk, A. Evaluation of cutting forces in granite treated with microwaves on the basis of multiple linear regression analysis. *Int. J. Rock Mech. Min. Sci.* **2018**, *107*, 69–74. [[CrossRef](#)]
25. Lu, J.; Xie, H.P.; Li, M.H.; Li, C.B.; Gao, M.Z.; Shang, D.L.; Li, J.H. Effect of microwave radiation on mechanical behaviors of tight fine sandstone subjected to true triaxial stress. *Int. J. Rock Mech. Min. Sci.* **2022**, *152*, 105063. [[CrossRef](#)]
26. Sun, W.; Ling, J.; Huo, J.; Guo, L.; Zhang, X.; Deng, L. Dynamic characteristics study with multidegree-of-freedom coupling in TBM cutterhead system based on complex factors. *Math. Probl. Eng.* **2013**, *3*, 635809. [[CrossRef](#)]
27. Li, X.B.; Gong, F.Q. Research progress and prospect of deep rock mechanics based on coupled static dynamic loading testing. *J. China Coal Soc.* **2021**, *6*, 846–866.
28. Li, X.B.; Lok, T.S.; Zhao, J. Dynamic characteristics of granite subjected to intermediate loading rate. *Rock Mech. Rock Eng.* **2005**, *38*, 21–39. [[CrossRef](#)]
29. Wang, P.; Yin, T.B.; Li, X.B.; Zhang, S.S.; Bai, L. Dynamic properties of thermally treated granite subjected to cyclic impact loading. *Rock Mech. Rock Eng.* **2019**, *52*, 991–1010. [[CrossRef](#)]
30. Li, X.; Wang, S.; Xu, Y.; Yao, W.; Xia, K.; Lu, G. Effect of microwave irradiation on dynamic mode-I fracture parameters of Barre granite. *Eng. Fract. Mech.* **2020**, *224*, 106748. [[CrossRef](#)]
31. Li, X.; Wang, S.; Xia, K.; Tong, T. Dynamic tensile response of a microwave damaged granitic rock. *Exp. Mech.* **2021**, *61*, 461–468. [[CrossRef](#)]
32. Wong, L.N.Y.; Maruvanchery, V.; Liu, G. Water effects on rock strength and stiffness degradation. *Acta Geotech.* **2016**, *11*, 713–737. [[CrossRef](#)]
33. Tang, S.B. The effects of water on the strength of black sandstone in a brittle regime. *Eng. Geol.* **2018**, *239*, 167–178. [[CrossRef](#)]
34. Peinsitt, T.; Kuchar, F.; Hartlieb, P.; Moser, P.; Kargl, H.; Restner, U.; Sifferlinger, N.A. Microwave heating of dry and water saturated basalt, granite and sandstone. *Int. J. Min. Min. Eng.* **2010**, *2*, 18–29. [[CrossRef](#)]
35. Kim, S.; Santamarina, J.C. Rock crushing using microwave pre-treatment. In Proceedings of the Geo-Chicago, Chicago, IL, USA, 14–18 August 2016; pp. 720–729.
36. Zhao, Q.H.; Zhao, X.B.; Zheng, Y.L.; Li, J.C.; He, L.; He, J.L.; Zou, C.J. Heating characteristics of igneous rock-forming minerals under microwave irradiation. *Int. J. Rock Mech. Min. Sci.* **2020**, *135*, 104519. [[CrossRef](#)]
37. Ahmadi, S.; Khormali, A.; Khouitori, F.M. Optimization of the demulsification of water-in-heavy crude oil emulsions using response surface methodology. *Fuel* **2022**, *323*, 124270. [[CrossRef](#)]
38. Lu, G.; Li, Y.; Hassani, F.; Zhang, X. The influence of microwave irradiation on thermal properties of main rock-forming minerals. *Appl. Therm. Eng.* **2017**, *112*, 1523–1532. [[CrossRef](#)]
39. Wang, S.; Xu, Y.; Xia, K.W.; Tong, T.Y. Dynamic fragmentation of microwave irradiated rock. *J. Rock Mech. Geotech. Eng.* **2021**, *13*, 300–310. [[CrossRef](#)]
40. Yin, T.B.; Wu, B.Q.; Wang, C.; Wu, Y. Determination of dynamic tensile strength of microwave-induced basalt using Brazilian test. *Rock Mech. Rock Eng.* **2022**, *55*, 1429–1443. [[CrossRef](#)]
41. Chen, J.H.; Althaus, S.M.; Liu, H.H.; Zhang, J.L.; Eppler, G.; Duncan, J.C.; Sun, Q.S. Electromagnetic-heating enhancement of source rock permeability for high recovery. *Fuel* **2021**, *283*, 118976. [[CrossRef](#)]
42. Li, H.; Lin, B.; Chen, Z.; Hong, Y.D.; Zheng, C.S. Evolution of coal petrophysical properties under microwave irradiation stimulation for different water saturation conditions. *Energy Fuels* **2017**, *31*, 8852–8864. [[CrossRef](#)]
43. Zhou, Y.X.; Xia, K.W.; Li, X.B.; Li, H.B.; Ma, G.W.; Zhao, J.; Zhou, Z.L.; Dai, F. Suggested methods for determining the dynamic strength parameters and mode-I fracture toughness of rock materials. *Int. J. Rock Mech. Min. Sci.* **2012**, *49*, 105–112. [[CrossRef](#)]
44. ISRM. Suggested methods for determining tensile strength of rock materials. *Int. J. Rock Mech. Min. Sci. Geomech. Abstr.* **1978**, *15*, 99–103. [[CrossRef](#)]
45. Xia, K.W.; Yao, W. Dynamic rock tests using split Hopkinson (Kolsky) bar system—A review. *J. Rock Mech. Geotech. Eng.* **2015**, *7*, 27–59. [[CrossRef](#)]
46. Li, X.B.; Zou, Y.; Zhou, Z.L. Numerical simulation of the rock SHPB test with a special shape striker based on the discrete element method. *Rock Mech. Rock Eng.* **2014**, *47*, 1693–1709. [[CrossRef](#)]
47. Dai, F.; Huang, S.; Xia, K.W.; Tan, Z.Y. Some fundamental issues in dynamic compression and tension tests of rocks using split Hopkinson pressure bar. *Rock Mech. Rock Eng.* **2010**, *43*, 657–666. [[CrossRef](#)]
48. Zhang, Q.B.; Zhao, J. A review of dynamic experimental techniques and mechanical behaviour of rock materials. *Rock Mech. Rock Eng.* **2014**, *47*, 1411–1478. [[CrossRef](#)]
49. Zhang, Z.X.; Yu, J.; Kou, S.Q.; Lindqvist, P.A. Effects of high temperatures on dynamic rock fracture. *Int. J. Rock Mech. Min. Sci.* **2001**, *38*, 211–225. [[CrossRef](#)]
50. Nelson, S.; Lindroth, D.; Blake, R. Dielectric properties of selected and purified minerals at 1 to 22 GHz. *J. Microw. Power Electromagn. Energy* **1989**, *24*, 213–220. [[CrossRef](#)]
51. Church, R.H.; Webb, W.E.; Salsman, J.B. *Dielectric Properties of Low-Loss Minerals*; US Department of the Interior: Washington, DC, USA, 1988; Volume 9194.

52. Xue, D.J.; Zhou, H.W.; Liu, Y.T.; Deng, L.S.; Zhang, L. Study of drainage and percolation of nitrogen–water flooding in tight coal by NMR imaging. *Rock Mech. Rock Eng.* **2018**, *51*, 3421–3437. [[CrossRef](#)]
53. Lai, J.; Wang, G.W.; Wang, Z.Y.; Chen, J.; Pang, X.J.; Wang, S.C.; Zhou, Z.L.; He, Z.B.; Qin, Z.Q.; Fan, X.Q. A review on pore structure characterization in tight sandstones. *Earth-Sci. Rev.* **2018**, *177*, 436–457. [[CrossRef](#)]
54. Weng, L.; Wu, Z.J.; Li, X.B. Mesodamage characteristics of rock with a pre-cut opening under combined static–dynamic loads: A nuclear magnetic resonance (NMR) investigation. *Rock Mech. Rock Eng.* **2018**, *51*, 2339–2354. [[CrossRef](#)]
55. Metaxas, A.C.; Meredith, R.J. *Industrial Microwave Heating*; Peter Peregrinus Ltd.: London, UK, 1983.
56. Rostásy, F.S.; Weiß, R.; Wiedemann, G. Changes of pore structure of cement mortars due to temperature. *Cem. Concr. Res.* **1980**, *10*, 157–164. [[CrossRef](#)]
57. Xie, K.N.; Jiang, D.Y.; Sun, Z.G.; Chen, J.; Zhang, W.G.; Jiang, X. NMR, MRI and AE statistical study of damage due to a low number of wetting–drying cycles in sandstone from the three gorges reservoir area. *Rock Mech. Rock Eng.* **2018**, *51*, 3625–3634. [[CrossRef](#)]
58. Li, J.L.; Kaunda, R.B.; Zhou, K.P. Experimental investigations on the effects of ambient freeze-thaw cycling on dynamic properties and rock pore structure deterioration of sandstone. *Cold Reg. Sci. Technol.* **2018**, *154*, 133–141. [[CrossRef](#)]
59. Hariti, Y.; Hader, A.; Faraji, H.; Boughaleb, Y. Scaling Law of Permeability and Porosity for Fluid Transport Phenomena in Porous PCM Media. *J. Appl. Comput. Mech.* **2021**, *7*, 84–92.
60. Wang, P.; Xu, J.; Liu, S. Ultrasonic method to evaluate the residual properties of thermally damaged sandstone based on time–frequency analysis. *Nondestruct. Test. Eval.* **2015**, *30*, 74–88. [[CrossRef](#)]
61. Liu, S.; Xu, J. An experimental study on the physico-mechanical properties of two post-high-temperature rocks. *Eng. Geol.* **2015**, *185*, 63–70. [[CrossRef](#)]
62. Köken, E. Estimation of deformation modulus of coals using artificial neural networks (ANN). *Acta Tech. Jaurinensis* **2022**, *15*, 125–129. [[CrossRef](#)]
63. Rubin, A.M.; Ahrens, T.J. Dynamic tensile failure induced velocity deficits in rock. *Geophys. Res. Lett.* **1991**, *18*, 219–222. [[CrossRef](#)]
64. Zhao, J.; Li, H.B. Experimental determination of dynamic tensile properties of a granite. *Int. J. Rock Mech. Min. Sci.* **2000**, *37*, 861–866. [[CrossRef](#)]
65. Wu, B.B.; Chen, R.; Xia, K.W. Dynamic tensile failure of rocks under static pre-tension. *Int. J. Rock Mech. Min. Sci.* **2015**, *80*, 12–18.
66. Weng, L.; Wu, Z.; Liu, Q.; Wang, Z. Energy dissipation and dynamic fragmentation of dry and water-saturated siltstones under sub-zero temperatures. *Eng. Fract. Mech.* **2019**, *220*, 106659. [[CrossRef](#)]
67. Li, J.; Rong, L.; Li, H.; Hong, S. An SHPB test study on stress wave energy attenuation in jointed rock masses. *Rock Mech. Rock Eng.* **2019**, *52*, 403–420. [[CrossRef](#)]
68. Haque, K. Microwave energy for mineral treatment processes—A brief review. *Int. J. Miner. Process.* **1999**, *57*, 1–24. [[CrossRef](#)]
69. Li, H.; Shi, S.; Lin, B.; Lu, J.; Lu, Y.; Ye, Q.; Wang, Z.; Hong, Y.; Zhu, X. A fully coupled electromagnetic, heat transfer and multiphase porous media model for microwave heating of coal. *Fuel Process. Technol.* **2019**, *189*, 49–61. [[CrossRef](#)]
70. Buck, A.L. *Buck Research CR-1A User's Manual*; Buck Research Instruments: Boulder, CO, USA, 1996.
71. Gulati, T.; Zhu, H.C.; Datta, A.K. Coupled electromagnetics, multiphase transport and large deformation model for microwave drying. *Chem. Eng. Sci.* **2016**, *156*, 206–228. [[CrossRef](#)]
72. Wang, F.; Konietzky, H. Thermo-mechanical properties of granite at elevated temperatures and numerical simulation of thermal cracking. *Rock Mech. Rock Eng.* **2019**, *52*, 3737–3755. [[CrossRef](#)]
73. Antao, S.M. Quartz: Structural and thermodynamic analyses across the $\alpha \leftrightarrow \beta$ transition with origin of negative thermal expansion (NTE) in β quartz and calcite. *Acta Crystallogr. Sect. B Struct. Sci. Cryst. Eng. Mater.* **2016**, *72*, 249–262. [[CrossRef](#)]
74. Heuze, F.E. High-temperature mechanical, physical and thermal properties of granitic rocks—A review. *Int. J. Rock Mech. Min. Sci. Geomech. Abstr.* **1983**, *20*, 3–10. [[CrossRef](#)]
75. Yin, T.B.; Zhuang, D.D.; Li, Q.; Tan, X.S.; Wu, Y. Effect of oxygen on damage mechanism and mechanical properties of sandstone at high temperature. *Bull. Eng. Geol. Environ.* **2021**, *80*, 6047–6064. [[CrossRef](#)]

Disclaimer/Publisher's Note: The statements, opinions and data contained in all publications are solely those of the individual author(s) and contributor(s) and not of MDPI and/or the editor(s). MDPI and/or the editor(s) disclaim responsibility for any injury to people or property resulting from any ideas, methods, instructions or products referred to in the content.